

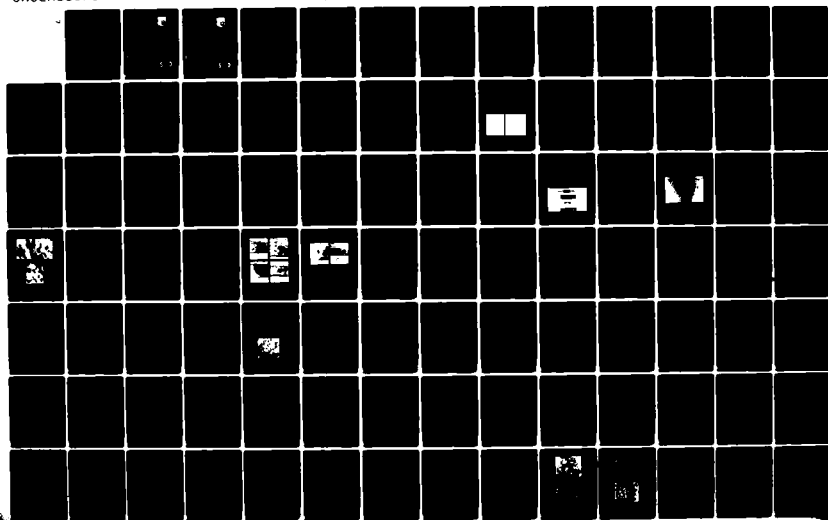
AD-A141 946

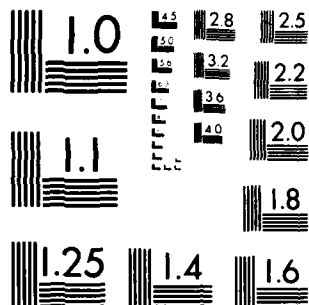
CHARACTERIZATION OF THE MICROSTRUCTURES OF VARIOUS
MATERIALS(U) SYSTEMS RESEARCH LABS INC DAYTON OH
RESEARCH APPLICATIONS DIV A G JACKSON ET AL. APR 84
AFWAL-TR-84-4052 F33615-80-C-5079 F/G 11/6

1/2

UNCLASSIFIED

NL





MICROCOPY RESOLUTION TEST CHART
NATIONAL BUREAU OF STANDARDS 1963-A

12

AFWAL-TR-84-4052

CHARACTERIZATION OF THE MICROSTRUCTURES
OF VARIOUS MATERIALS



A. G. Jackson
E. Omlor
E. Harper
J. Bacon
D. Brodecki

Research Applications Division
Systems Research Laboratories, Inc.
2800 Indian Ripple Road
Dayton, Ohio 45440-3696

April 1984

Final Report for Period 1 September 1980 - 31 August 1983

Approved for public release; distribution unlimited.

MATERIALS LABORATORY
AIR FORCE WRIGHT AERONAUTICAL LABORATORIES
AIR FORCE SYSTEMS COMMAND
WRIGHT-PATTERSON AIR FORCE BASE, OH 45433

DTIC
ELECTE
JUN 12 1984
S E D

84 06 11 002

DTIC FILE COP AD-A141 946

12

AFWAL-TR-84-4052

CHARACTERIZATION OF THE MICROSTRUCTURES
OF VARIOUS MATERIALS



A. G. Jackson
L. E. Omlor
L. E. Harper
L. J. Bacon
L. D. Brodecki

Research Applications Division
Systems Research Laboratories, Inc.
2800 Indian Ripple Road
Dayton, Ohio 45440-3696

April 1984

Final Report for Period 1 September 1980 - 31 August 1983

Approved for public release; distribution unlimited.

MATERIALS LABORATORY
AIR FORCE WRIGHT AERONAUTICAL LABORATORIES
AIR FORCE SYSTEMS COMMAND
WRIGHT-PATTERSON AIR FORCE BASE, OH 45433

DTIC
ELECTE
JUN 12 1984
S E D

84 06 11 002

DTIC FILE COP AD-A141 946

NOTICE

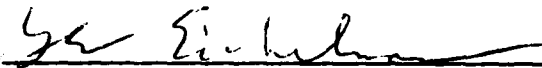
When Government drawings, specifications, or other data are used for any purpose other than in connection with a definitely related Government procurement operation, the United States Government thereby incurs no responsibility nor any obligation whatsoever; and the fact that the government may have formulated, furnished, or in any way supplied the said drawings, specifications, or other data, is not to be regarded by implication or otherwise as in any manner licensing the holder or any other person or corporation, or conveying any rights or permission to manufacture use, or sell any patented invention that may in any way be related thereto.

This report has been reviewed by the Office of Public Affairs (ASD/PA) and is releasable to the National Technical Information Service (NTIS). At NTIS, it will be available to the general public, including foreign nations.

This technical report has been reviewed and is approved for publication.



CHARLES R. UNDERWOOD
Manager, Characterization Facility
Structural Metals Branch
Metals & Ceramics Division
FOR THE COMMANDER



GAIL E. EICHELMAN
Chief, Structural Metals Branch
Metals & Ceramics Division

"If your address has changed, if you wish to be removed from our mailing list, or if the addressee is no longer employed by your organization please notify AFWAL/MLLS W-PAFB, OH 45433 to help us maintain a current mailing list".

Copies of this report should not be returned unless return is required by security considerations, contractual obligations, or notice on a specific document.

Unclassified

SECURITY CLASSIFICATION OF THIS PAGE

AD-A41946

REPORT DOCUMENTATION PAGE

1a. REPORT SECURITY CLASSIFICATION Unclassified			1b. RESTRICTIVE MARKINGS									
2a. SECURITY CLASSIFICATION AUTHORITY			3. DISTRIBUTION/AVAILABILITY OF REPORT Approved for public release; distribution unlimited									
2b. DECLASSIFICATION/DOWNGRADING SCHEDULE												
4. PERFORMING ORGANIZATION REPORT NUMBER(S) 6601 Final			5. MONITORING ORGANIZATION REPORT NUMBER(S) AFWAL-TR-84-4052									
6a. NAME OF PERFORMING ORGANIZATION Systems Research Labs., Inc.		6b. OFFICE SYMBOL (If applicable)	7a. NAME OF MONITORING ORGANIZATION AFWAL/MLLS									
6c. ADDRESS (City, State and ZIP Code) 2800 Indian Ripple Rd. Dayton, OH 45440-3696			7b. ADDRESS (City, State and ZIP Code) Material Laboratory (AFWAL/MLLS) Wright-Patterson Air Force Base, OH 45433									
8a. NAME OF FUNDING/SPONSORING ORGANIZATION		8b. OFFICE SYMBOL (If applicable)	9. PROCUREMENT INSTRUMENT IDENTIFICATION NUMBER F-33615-80-C-5079									
8c. ADDRESS (City, State and ZIP Code)			10. SOURCE OF FUNDING NOS.									
			<table border="1"><tr><td>PROGRAM ELEMENT NO.</td><td>PROJECT NO.</td><td>TASK NO.</td><td>WORK UNIT NO.</td></tr><tr><td>62102F</td><td>2418</td><td>2</td><td>12</td></tr></table>		PROGRAM ELEMENT NO.	PROJECT NO.	TASK NO.	WORK UNIT NO.	62102F	2418	2	12
PROGRAM ELEMENT NO.	PROJECT NO.	TASK NO.	WORK UNIT NO.									
62102F	2418	2	12									
11. TITLE (Include Security Classification) Characterization of the Microstructures of Various Materials												
12. PERSONAL AUTHOR(S) Jackson, A. G., Omlor, R. E., Harper, C. E., Bacon, R. J., and Brodecki, K. D.												
13a. TYPE OF REPORT Final		13b. TIME COVERED FROM 1/9/80 TO 31/8/83		14. DATE OF REPORT (Yr., Mo., Day) APRIL 1984								
15. PAGE COUNT 100												
16. SUPPLEMENTARY NOTATION												
17. COSATI CODES			18. SUBJECT TERMS (Continue on reverse if necessary and identify by block number)									
FIELD	GROUP	SUB. GR.										
11	04		Electron optics, TEM/STEM, SEM, microprobe, optical microscopy, Al, Ti, polymers, microtomy, rapid solidification									
11	06											
19. ABSTRACT (Continue on reverse if necessary and identify by block number) Research on characterization of microstructures of alloys and non-metallic materials is summarized. The emphasis was on improvements in the appreciation of electron-optical and optical-microscopy methods for determining the morphology, crystallography, and composition of the materials. Alloys studied included those of Al, Ti, and Ni base prepared by ingot, cast, and rapid-solidification methods. Non-metals were polymers and composites of various formulations. Accomplishments included installation of a scanning transmission electron microscope with energy dispersive spectrometry and electron energy loss spectrometers, installation of an ultramicrotome for preparation of non-metallic specimens, development and improvement of specimen-preparation techniques applied to non-metallics, metal powders, and metallurgical specimens, documentation of microstructures, formulation of analytical methods to provide compositional data, and construction of a simple apparatus for generating experimental quantities of rapidly solidified alloys. Papers and presentations authored or co-authored by personnel are listed.												
20. DISTRIBUTION/AVAILABILITY OF ABSTRACT UNCLASSIFIED, UNLIMITED <input checked="" type="checkbox"/> SAME AS RPT. <input type="checkbox"/> DTIC USERS <input type="checkbox"/>			21. ABSTRACT SECURITY CLASSIFICATION Unclassified									
22a. NAME OF RESPONSIBLE INDIVIDUAL C. R. Underwood			22b. TELEPHONE NUMBER (Include Area Code) 513-255-4018	22c. OFFICE SYMBOL AFWAL/MLLS								

PREFACE

This final report was prepared by the Research Applications Division of Systems Research Laboratories, Inc., 2800 Indian Ripple Road, Dayton, OH 45440-3696, under Contract No. F33615-80-C-5079, Project 2418, Task 2, Work unit 12, with Mr. Charles Underwood (AFWAL/MLLS) as Government Project Monitor. The research was under the general direction of Dr. Allen G. Jackson who served as Principal Investigator and Program Manager.

This report, submitted in December 1983, describes research accomplished during the period 1 September 1980 through 31 August 1983.

Accession For	
NTIS GRA&I	<input checked="checked" type="checkbox"/>
DTIC TAB	<input type="checkbox"/>
Unannounced	<input type="checkbox"/>
Justification	
By _____	
Distribution/ _____	
Availability Codes	
Dist	Avail and/or Special
A-1	




TABLE OF CONTENTS

SECTION	PAGE
1 INTRODUCTION	1
2 SUMMARY OF WORK PERFORMED	5
ELECTRON-OPTICS	5
New Equipment	5
New Techniques	9
SCANNING ELECTRON MICROSCOPY	15
Selected-Area Channeling	15
New Equipment and Methods Developed	16
ELECTRON MICROPROBE ANALYSIS	17
METALLOGRAPHY, PHOTOGRAPHY, AND HEAT TREATMENT LABORATORIES	23
New Equipment	23
New Techniques	24
Evaluation of Automatic Polishing and Grinding Systems	31
SPECIAL PROJECTS	33
Pendant Drop Melt Extraction (PDME) Ti Ribbon	33
Types of Cooling Produced by Rapid- Solidification-Technology (RST) Ribbon	40
Calculations of Weight Percent of Constituents in Ge Precipitate in Alloy With 7.5 Weight Percent Ge Aged for 40 hr. at 535°C	45
3 PAPERS, PRESENTATIONS, EXHIBITS, MEETINGS, AND SCHOOLING	58
REFERENCES	66
APPENDIX	67

LIST OF ILLUSTRATIONS

FIGURE		PAGE
1	Nickel Electroplating Technique for Metal-Alloy Powders. (a) Electroplating Set-up, (b) P&W RSR185 Ni-Ni Plate, (c) Powder Distribution in 3-mill Disk.	12
2	Schematic Representation of Voltage-Current Characteristics for Electropolishing Solutions.	13
3	Short-Crack Fatigue Samples, As-Received and After Removal of 0.38 mm of Material by Electrolytic Polish.	27
4	Residual Surface Stress Measured on Carefully Milled Ti-6246 Surface as Function of Depth of Material Removed by Polish.	28
5	Micrograph Revealing True Microstructure of Ti-6246 After Electrolytic Polish. Magnification 60 \times under polarized light.	29
6	(a) Ti-10V-1Fe-3Al Microstructure Revealing Deformed Grains in Matrix (30% Reduction) at 925°C. (b) Recrystallized Grain Structure Superimposed with Image of Original Deformed Grain Structure in Annealed and Quenched Specimen. (c) Recrystallized Grain in Annealed and Quenched Specimens After Removal of Deformed-Grain "Ghost" Boundaries. Magnification 4 \times .	32
7	SEM Micrographs of CP Ti PDME Ribbon Produced at Various Rotational Speeds. (a) Side View, (b) Three-Quarter View.	34
8	SEM Micrographs of CP Ti PDME Ribbon Produced at Various Rotational Speeds. (a) 1400 RPM, (b) 2000 RPM, (c) 2100 RPM (d) 2850 RPM, (e) 3000 RPM, (f) 3600 RPM.	36
9	Plot of Wheel Tangential Velocity as Function of Rotational Speed for PDME Apparatus.	38
10	Ribbon-Thickness Data Plotted as Function of Wheel Rotational Speed. Scatter in data arose from sampling of ribbon which had not reached stability when formed.	39
11	Plot of Cooling Rate vs. Time for Dimensionless Variables Used by Katgerman (Redrawn Fig. 2 from Ref. 8).	43
12	Regions of foil with Precipitate (1) and Without Precipitate (2).	48
13	STEM Micrograph of Area From Which Intensity Measurements Listed in Table 7 Were Made.	50

LIST OF ILLUSTRATIONS (CONT'D.)

APPENDIX FIGURE		PAGE
1	Area Fraction Versus Sintering Time at 1315°C for Base Alloy.	80
2	Area Fraction Versus Sintering Time for Base Alloy With Various Amounts of Si.	81
3	Area Fraction Versus Sintering Time for Base Alloy With Various Amounts of Ge.	82
4	Porosity Obtained in Base + 0.1 wt. pct. Si Alloy: (a) As-Received, (b) After 10 hr. at 1315°C, (c) After 30 hr., (d) After 50 hr.	83
5	Grain Size (mm/Grain) Versus Sintering Time for Base Alloy.	85
6	Grain Size (mm/Grain) Versus Sintering Time for Si Containing Alloys.	86
7	Grain Size (mm/Grain) Versus Sintering Time for Ge Containing Alloys.	87
8	Microstructures Obtained in Base + 0.1 wt. pct. Si Alloy: (a) As-Received, (b) After 10 hr. at 1315°C, (c) After 30 hr., (d) After 50 hr.	88

LIST OF TABLES

TABLE	PAGE
1 Transmission and Scanning Transmission Microscopy and Microtomy	5
2 Summary of EPMA Support	17
3 Summary of Support Activities	23
4 Nusselt Numbers for Various Values of Heat-Transfer Coefficient, h , and Thickness, d	41
5 Dimensionless Time as a Function of h and t for Ti and for Al	41
6 Contributions to Measured Intensity	47
7 Results of Calculations of Ti and Ge Present in Precipitates using Cliff-Lorimer Method	51
8 Results of Calculations of Ti and Ge Present in Precipitate using Zaluzec Method	51

APPENDIX TABLE

1 Weight Percent of Components in Alloys Studied	71
---	----

Section I

INTRODUCTION

New and improved materials are being studied by the AFWAL Materials Laboratory to determine their usefulness in Air Force systems. Improved properties, reduced costs, processing simplifications, and enhanced service life are several of the driving forces in the search for improved materials. A significant part of this search involves characterization of the microstructures of materials being developed for use in aerospace systems.

Techniques for characterizing materials have become very sophisticated, requiring strong interaction between materials engineers and specialists in the use of characterization techniques. Each scientist and engineer at the AFWAL Materials Laboratory who is involved in the development and evaluation of materials has characterization problems unique to the material and properties under study. In recognition of these problems, the Materials Laboratory established the Materials Characterization Facility where research related to characterization could be conducted.

Requirements for more sophisticated methods of characterization have arisen from the on-going refinement of operational demands on Air Force systems. For example, the current Air Force philosophy and approach to providing structural safety and durability in military aircraft were fostered by the high-cost, late systems-development programs. These programs led to increased in-service maintenance and modification costs and, in some cases, less-than-desirable fracture resistance of the structures.

Implementation of this philosophy is carried out using, for example, Specification MIL-A-83444¹ which establishes damage-tolerance requirements based on defects or flaws which are assumed to be present in the

structural material, possibly as a result of component processing or fabrication. The design of the component must be based upon load and the size and location of the flaw. Also inspection intervals for the structure depend upon the growth limits, in terms of flight time, to a defect attaining critical size.

Another specification, MIL-A-8867,² establishes durability requirements to insure that the economic life of the structure will be equal to or greater than the specified design service life when the structure is subjected to the design service loads. The economic life refers to the life of a structure which has sufficient widespread damage to preclude its operation and to render it economically beyond repair. In an evaluation of durability, design procedures must take into account the growth of cracks under design loads and environmental spectra and insure that cracks will not grow to sizes which necessitate replacement or modification of components in the required design life. This continuous need for more reliable structural materials and methods of predicting material behavior under service conditions has placed challenging demands upon materials scientists and engineers who are seeking the thorough understanding of fundamental material properties which is essential in the development and evaluation of materials for Air Force use.

Alloys of aluminum and titanium, nickel-base superalloys, nonmetallic materials, and composites are of major significance relative to the mission of the Air Force. Research on high-strength aluminum alloys has now encompassed most of the compositions that can be made using standard melting, ingot casting, and work processes. There is considerable evidence that emerging powder technology will lead to alloys having improved combinations of strength, toughness, and stress-corrosion resistance, as compared to current alloys, and perhaps even improved fatigue properties. Associated with these new alloys, however, is a class of microstructures not found in conventional alloys, and their role in controlling properties has not been established.

One of the aims of the research being conducted at the AFWAL Materials Laboratory is examination of microstructure/property relationships in order to anticipate possible problems associated with the aluminum powder-technology area. Such examination involves assessing the role of the various microstructural features peculiar to powder alloys in light of their effect upon the critical reliability properties of fatigue-crack-growth rate, toughness, and stress-corrosion resistance.

In continuing efforts to improve titanium alloys with respect to performance, reliability, cost, and producibility, the influence of metallurgical variables upon properties is determined to permit proper manipulation of processing and composition which, in turn, permits the desired properties to be obtained most effectively. The AFWAL Materials Laboratory effort involves utilizing relationships between the properties and microstructure of titanium alloys to develop those processes, heat treatments, and minor alloying changes which reduce property scatter as well as improve mean values. The activity centers around fatigue and creep properties; but, by necessity, other properties are included in order to obtain base-line data.

The utilization of ceramics in turbine engines offers significant potential for increased efficiency and lower cost. Recognizing this, the Air Force established the Interagency Coordination Group for the Application of Ceramic to Turbine Engines to develop an interdependent program as a means of maximizing accomplishments. It was agreed that the Air Force would evaluate new materials developed by other organizations and also carry out screening and characterization for the component programs of other organizations. The Materials Laboratory activity covers the area of microstructural characterization and that area of mechanical behavior which is critical to the application of ceramics to turbines.

The SRL program on microstructural characterization complemented AFWAL Materials Laboratory in-house R&D work in the above areas. Unique equipment and specialized investigative techniques used were peculiar to this laboratory and included optical metallography, electron microscopy, quantitative metallography, and heat treatments--all requiring

application of standard specimen-preparation methods and variations of these methods. The program provided the flexibility and versatility required for accomplishment of objectives in cooperation with the inherently diverse, exploratory, and probing nature of the Materials Laboratory effort. To meet these goals effectively, the program was performed on-site at the AFWAL Materials Laboratory, most of the work being concurrent and integrated with on-going investigations on materials in this as well as other AFWAL laboratories.

Materials on which characterization was accomplished included metals and nonmetals such as ceramics, carbon filaments, boron-titanium-silicon composites, and polymers. Alloys included those of aluminum and titanium and nickel-base superalloys.

The following personnel were assigned to this effort:

Project Manager/Principal Investigator	Dr. A. G. Jackson
Assistant Project Manager/TEM	R. E. Omlor
Microtomy	P. F. Lloyd
SEM	J. Y. L. Chen/R. J. Bacon/R. L. Brodecki
EPMA	M. B. Strope/R. J. Bacon/ A. G. Jackson
Metallography Lab	W. J. Custer/C. E. Harper/ F. O. Deutscher/R. K. Lewis
Photo Lab	J. C. Heidenreich/S. D. Apt
Special Projects	J. G. Paine
Technical Support	J. S. Paine

The conscientious effort of this staff in producing high-quality data and analyses is gratefully acknowledged.

Section 2
SUMMARY OF WORK PERFORMED

ELECTRON-OPTICS

R. E. Omlor

The following table represents the total number of samples prepared and photographs taken in the TEM and STEM areas.

TABLE 1 TRANSMISSION AND SCANNING TRANSMISSION MICROSCOPY AND MICROTOMY			
Samples Prepared		Photographs Taken	
Al Foils	1,545	TEM (200 kV)	6,677
Ti Foils	1,675	TEM (STEM-100CX)	12,729
Ni Foils	114	SEM-STEM (100CX)	3,264
Ocean Ion Mill	105		
Microtome 306 specimens, (3 each)	1,188		

New Equipment

100 X JEOL STEM

During the course of this contractual effort, many advances were made in the application of electron optics for characterization of materials under study in the Materials Laboratory, the most significant being the installation of the 100CX JEOL Scanning Transmission Electron Microscope (STEM). This analytical microscope has not only the capability to perform the usual tasks of conventional TEMs, SEMs, and electron microprobes but also two distinct additional capabilities--microdiffraction and microanalysis.

Because of the small-diameter ($\sim 10 \text{ \AA}$) electron beam, diffraction from extremely small areas can be achieved. If the gun bias control is employed, the probe size and current density can be adjusted easily.

Also, the probe can be scanned over a limited region, providing micro-area selected diffraction with no undesirable radiation damage to adjacent areas. The small electron beam can also be used as a super-fine electron probe to generate characteristic x-rays and, when coupled with an x-ray detector, can provide chemical species identification of a spatial region on the order of ten times the probe diameter--a much smaller area than possible with a conventional microprobe. Concentration profiles can be obtained as the beam traverses the sample. With the electron-energy-loss spectrometer (EELS), which utilizes the same analysis system as the x-ray analyzer, micro-elemental analysis and imaging for the light elements (down to Li) can be performed, either in addition to or simultaneous with x-ray microanalysis. Furthermore, the analytical instrument can provide a TEM-mode high-resolution ($\sim 2 \text{ \AA}$) image of the specimen area under investigation. Thus, this single instrument approaches the ultimate in analytical capabilities.

Other accessories and capabilities of the 100CX JEOL STEM are:

1. Deformation sample holder for direct observation of sample stretching by any of the above techniques.
2. Hot- and cold-stage holders for observation of phase transitions and frozen samples and cooled polymer samples to reduce beam damage.
3. Free lens control for use with special bright-field/dark-field imaging techniques.
4. Raster scan imaging for use in secondary-electron imaging in the reflection mode (SEI, same as SEM), transmitted electron imaging (TEI) (unavailable in SEM), and back-scattered electron imaging (BEI) in the case of high-atomic-number elements.

Since a high-resolution dynamic image is available on a CRT, video-tape and digital-image-analysis capabilities are available for dynamic processes. The major advantage of the STEM is system flexibility.

TN-2000 X-ray Analyzer

A second related update was the acquisition of Tracor-Northern TN-2000 X-ray Analyzer and its related stand-alone unit. This unit provides digital beam automation, which permits imaging of both x-rays and various video signals. Digital beam control refers to automatic control and direction of the STEM electron beam by the TN-2000 Analyzer. Additionally, the standard video signal of the microscope is digitized and transmitted to the analyzer. Automation of the electron microscope with this integrated TN-2000 system provides several powerful capabilities:

1. High-quality digital x-ray maps and line scans
2. Particulate analysis
3. Feature analysis
4. Digital image analysis.

TN-1310 Modular Control

The Tracor-Northern TN-1310 Modular Control, in conjunction with the TN-2000 X-ray Analyzer, affords the JEOL 100CX STEM tremendous capabilities. The computer power of the x-ray analyzer is used to control electron beam scanning and CRT displays as well as to image video and x-ray signals digitally. The system enables positioning of the electron beam in the X and Y directions. With software programs point spacing and dwell time can be provided. The digital converter is used to digitize the video signals (secondary, backscattered and transmitted electrons) into 256 gray levels. The joystick is used to position the cursor on the microscope image, control brightness and contrast, select start and stop points for line profiles, and set threshold levels for particle detection.

Line Profiling: Seven background-subtracted line profiles can be collected simultaneously and displayed in color.

Distribution Mapping: Eight background subtracted maps can be collected simultaneously and displayed in color.

Transfer of Information to STEM CRT: Line profiles, distribution maps, EDS spectra, alphanumerics, a micron bar, and energy grids can be transferred to electron-microscope display and photo CRT.

Digital Imaging: Digital images of a variety of video signals (secondary and backscattered electrons, etc.) can be collected and displayed in sixteen colors and coded to intensity.

Image Processing: Image processing available includes background subtraction, composite, smoothing, rationing, threshold selection, scale expander, histogram, area fraction, and add/subtract.

In addition, two important sample-preparation devices were purchased--the Gatan Ion Mill and the Reichert-Jung Ultramicrotome. With the former device, two specimens can be prepared at one time. The stages insure that the ion beams are centered on the specimen over a full 40 degree range of sputtering angles. The rotatable stage includes the necessary ductwork for independent feeding of the ionizing gas to the two guns. Each milling area contains a high-voltage switch which enables the operator to energize one or both guns as well as a specimen area which provides (a) specimen rotation about the vertical axis (b) fast specimen exchange or cleaning capabilities without affecting the milling conditions of the twin milling station (c) transmission illumination viewing (d) a window for close specimen viewing, and (e) laser termination capabilities. High quality results have been obtained for scientists in both the metals and ceramics areas.

The design of the second sample-preparation device--the Reichert-Jung Ultramicrotome with cryo-microtome capabilities--simplifies the day-to-day preparation of sections. This unit features thermal feed and a

variable speed drive control with adjustment of the cutting range. It is also back-lighted to assist with correct knife setting in relation to the cutting surface of the specimen. With this instrument high-quality results have been obtained for the Polymer Branch of the AFWAL Materials Laboratory.

New Techniques

With the introduction of a wide variety of alloys of both titanium and aluminum, numerous small changes have been made under the present contract in foil-making processes. Various special foil-making techniques have also been developed for the Polymer Branch of the Air Force Wright Aeronautical Laboratories.

The use of composite materials in aerospace applications is increasing because of the significant weight, cost, and performance advantages which these materials have over conventional-strength materials. In the past, however, poor results have been obtained on sectioning graphite fiber-epoxy composites. It has become essential, therefore, to develop new techniques for sectioning these hard, brittle fibers. Many advances in microtomy resulted from the introduction of the Reichert-Jung Ultra-microtome. The knife angle can be changed from a low angle (45 deg.) to a high angle (55 to 60 deg.), depending on the specimen. The speed of cut can also be reduced to very slow. On the average, one specimen requires one to three days for cutting. These changes in technique resulted in the publication of five papers (see Section 3).

Structural adhesive bonding to oxidized aluminum wire (surface treated) was used to study the adhesive-adherence interaction at the interphase. The method of matching the hardness of the embedding media to that of the specimen produced excellent results (see Section 3, Paper No. 5).

Cured epoxy resin was thought to have a heterogeneous morphology comprised of spherical entities in the 5-50 μm range in a matrix of lower cross-link density. A combination of techniques was used to

investigate this. TEM studies were made on (a) microtomed sections both unstained and osmium-tetroxide stained along with x-ray mapping of osmium in the STEM (b) special replication techniques of unetched and argon-plasma-etched fracture surfaces, and (c) replicas (special techniques) of plasma-etched as-cured surfaces. This combination of techniques showed the heterogeneities to be spherical and have a size distribution (See Section 3, Paper Nos. 13 and 14).

In replication generally the surfaces of the cured samples or fracture surfaces, unetched or suitably etched, are examined in the TEM using the two-stage replica method. The replicating fluid commonly used is 25% polyacrylic acid (MW = 250,000) solution in water.^{3,4} This dries to a brittle replica which is removed by mechanical prying with the help of tweezers; extreme care is required to ensure that the replica is not damaged. It has been shown⁵ that for fractographic studies of epoxy resin, replication based on PAA can give rise to artifacts; hence, it is necessary to substantiate the results with other evidence, e.g., from the SEM. Although the standard replicating fluid which contains 10% cellulose acetate in acetone, gives a softer and more easily removable replica, the acetone can affect the surface of epoxy resin. To circumvent this problem, a modified replication method was developed and is described here.

The epoxy resin used was EPON 828 (Shell) which is based on diglycidyl ether of Bisphenol-A. It was cured with different amounts of meta-phenylene diamine, the stoichiometric amount being 14.5 parts per hundred parts by weight of the resin. The resin and the curing agent were mixed at 75°C, degassed under vacuum, and then cast into rectangular specimens in silicone rubber molds. These were cured for 2 hr. at 75°C, followed by 2 hr at 125°C. The samples were immersed in liquid nitrogen and fractured by bending. The fracture surfaces were then etched for 30 min. in a cold plasma using 50-W power at a flow rate of about 20 mL/min. of argon gas and a pressure of 0.5 mm mercury.

The plasma-etched fracture surface was placed about 13 cm directly below carbon electrodes in a vacuum coating unit, and a thin evaporated layer of carbon was deposited on the surface. It was expected that this thin

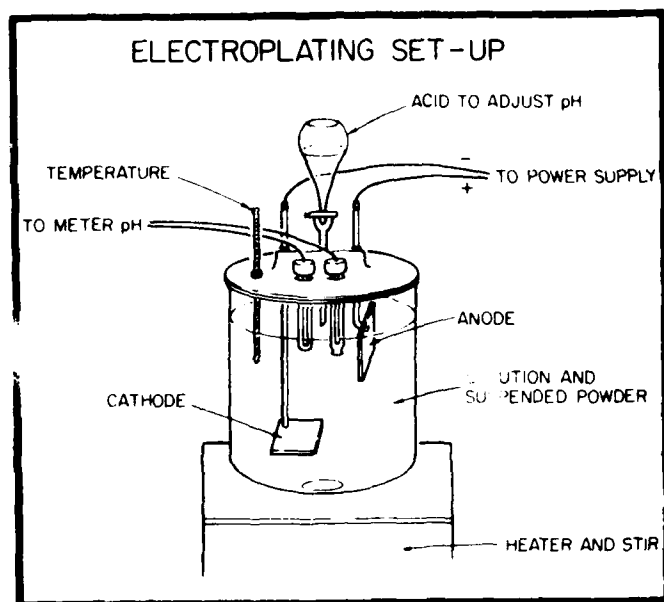
carbon film would not disturb the topography of the fracture surface and would act as a barrier to the diffusion of acetone onto the epoxy. The usual replication procedure was then followed, viz., the replicating fluid was applied to the carbon-coated fracture surface and the dried polymer film was peeled off. It was noted that, in general, the carbon layer remained intact on the sample when the cellulose-acetate replica was removed and that the sample was apparently not affected by acetone. Next a carbon-platinum film was evaporated onto the replica at an angle, and the film was supported by evaporating a carbon base onto the sample. After being mounted on a grid, the cellulose acetate was removed by dissolving in acetone and the replica was examined in a JEOL TEM-100 CX.

In the area of metals, many significant advances were also made. With increased interest in the use of prealloyed powder and ribbon, new techniques were required. The small particle size resulting from the powder-producing methods makes it difficult to prepare thin foils suitable for studies in the TEM which is a valuable tool for judging the level of supersaturation achieved within a given alloy system and provides information as to the identification, distribution, and crystallographic orientation of the non-equilibrium structures inherent in RST. The techniques which were improved upon are: (a) nickel-plating techniques, (b) jet acid thinning, (c) ion milling, and (d) microtomy. The application of the various methods depends upon the material used for securing the individual powder particles as well as the base metal of the particular powder type.

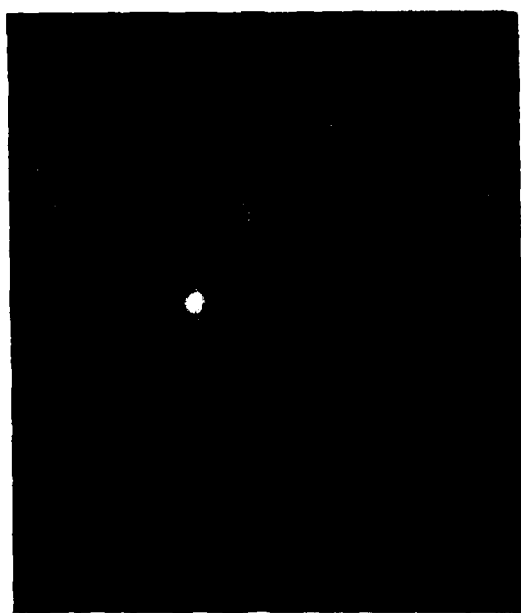
Nickel Plating

Powder particles must be embedded in a metal matrix which can be handled in the same way as a conventional foil. Therefore, a nickel-plating technique was developed. A solution was made of 350 g nickel sulphamate, 20 g boric acid, and 5 g nickel chloride in 500 ml of distilled H_2O .

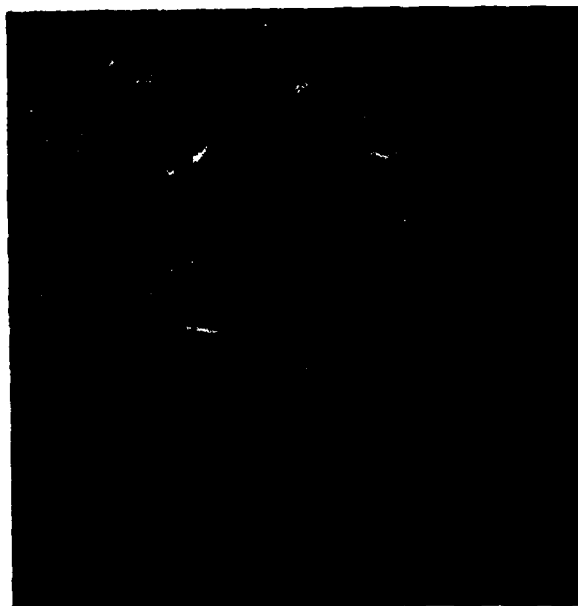
A pure nickel anode was used with the powder being placed on a stainless cathode. The process was carried out at $-60^\circ C$ with no stirring at 1 A in the 0 - 50 V range at 100 mA for a period of 6 hr. (see Fig. 1). This method yielded a workable foil which could be placed in the Ion Mill for polishing.



(a)



(b)



(c)

Figure 1. Nickel Electroplating Technique for Metal-Alloy Powders.
 (a) Electroplating Set-Up, (b) P&W RSR 185 Ni-Ni Plate,
 (c) Powder Distribution in 3-mill Disk

Jet Acid Thinning

With the wide variety of alloys presently being studied, constant changes are being made in the jet-acid thinning process. A standard solution (200 ml methanol, 150 ml butyl cellusolve, and 7 - 20 ml perchloric acid) must be modified daily according to the alloy to achieve desired results.

To establish the correct conditions for electropolishing, it is necessary to obtain the voltage-current relation for the electrolyte and specimen material being used (see Fig. 2). Conditions are monitored daily, and desired results have been obtained.

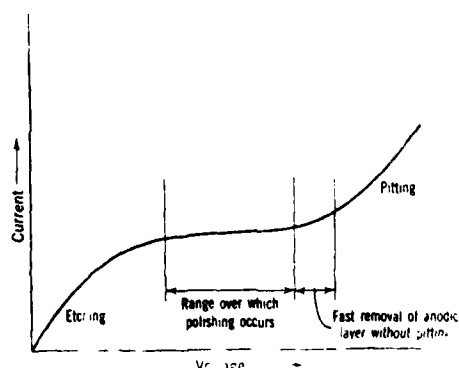


Figure 2. Schematic Representation of Voltage-Current Characteristics for Electropolishing Solutions [Transmission Electron Microscopy of Metals, ed. Gareth Thomas (John Wiley & Sons, Inc., New York, 1962), p. 152].

Ion Milling

Workable samples have also been made by ion milling. Several factors must be considered if ion milling is to be a success. First, the powder type must possess a sputtering rate comparable to or faster than that of the substrate material. A comparable sputtering rate can be achieved by electroplating similar materials. Problems may arise due to the difference in sputtering behavior caused by alloying additions to the powder. The difference in sputtering rate due to material differences may be advantageous, for example, in the preparation of a thin foil containing aluminum powder particles. The electroplating of a material with a known lower sputtering rate within the operational range of the milling device will result in the preferential thinning of the aluminum powder particles. Ion-milling techniques combined with nickel plating have produced excellent results.

Microtoming

The microtoming techniques were discussed in detail previously with reference to polymers. However, microtoming has also been utilized on various powders--especially aluminum. The microtome process for powder involves embedding the powder in an epoxy substrate of comparable hardness. Sections 700-Å thick are obtained using a diamond knife microtome with a 55 - 60 deg. angle cutting edge. The artifacts produced by this method are chattering lines, caused by the knife, and the introduction of dislocations due to bulk deformation of the powder particles (see Section 3, Paper Nos. 7, 11, and 12).

The above sample-preparation techniques are used on a daily basis in routine analyses.

SCANNING ELECTRON MICROSCOPY

R. D. Brodecki

During this reporting period 3,809 samples were evaluated, with 16,551 photographs and negatives being required. EDS analysis was generally requested, with digital Decwriter print-outs and color photographs of labeled spectra. Included in these efforts were sample preparation, carbon or gold palladium coating of samples, negative processing, and instrument rep .

Selected-Area Channeling

Instrument modifications required for selected-area electron channeling were complicated. After the SEM had been vented and shut down and the power turned off, the secondary detector was removed. A spacer was added to the secondary detector to make room for the electron-channeling detector. The right-side port plate was removed and the rocking coil assembly with detector mounted in place. Centering and alignment of the assembly to the final pole piece were crucial for achieving proper channeling patterns. At this point, cables were connected to the rocking coil assembly and to the rocking control module located in the NII bin. The next step involved the alignment procedure. The adjustments could not be used in all cases to correct the images, as outlined in the procedures. The adjustment on the rocking control module appeared to have little or no affect. After set-up and calibration were complete, the sample to be analyzed was inserted. After several unsuccessful attempts to achieve the correct pattern, the standard was re-inserted. At this time the channeling detector was discovered to be defective. Since the technique is time consuming and difficult and limits the instrument to electron channeling, further attempts seemed unjustified in view of the heavy demands for SEM.

Most scanning electron microscopes are equipped with an energy-dispersive x-ray spectrometer (EDS), for achieving quantitative results on a smooth-surface sample in a short period of time. However, a method was required for achieving the same results on a fracture sample. After

extensive research it was found that optimum results could be achieved by rotating and tilting the sample, with the sample being placed as close to the detector as possible and at an angle of ~ 30 deg. Subsequent data were of the same quality as those from a polished sample of the same material. Thus, once the correct angle relative to the detector and the correct degree of tilt have been determined, reliable data can be generated.

New Equipment Methods Developed

ETEC Autoscan Holder

A holder for 1.5-in. samples was devised suitable for use with the ETEC Autoscan sample stage. In the past when a mounted sample larger than 1 in. was to be examined, the sample was broken out of the mounting material or double-sided tape was placed on the bottom of the sample and copper tape extended from the sample down over the double-sided tape which secured the sample to the stage of the SEM. Since the bond was seldom secure, sample movement, picture graininess, poor conduction, and overall poor SEM quality resulted. With the development of the larger holder, such problems were eliminated and the quality and magnification capabilities of the larger samples increased.

Cleaning Procedure

The greatest hindrance to timely completion of projects was dirty samples. Inadequate cleaning procedures often resulted in chlorine, calcium, potassium, sulfur and silicon combinations being found in or around the initiation site, in stains in various locations on mounted, polished, and etched specimens, or in a film blanketing the surface. Thus, when attempts were made to photograph the specimen, charging and burning occurred which created unusable photographs. Also high resolution could not be achieved. The standard method of etching the specimen using sodium bicarbonate as reagent and then methanol and compressing or hot-air drying was found to be inadequate. On fracture

samples, the specimen after failure is sonicated in methanol and then compressed-air or hot-air dried--a procedure which was also determined to be inadequate. In most cases the elements mentioned recrystallized on the surface of the specimen instead of vaporizing. To eliminate this problem a longer, but more effective, procedure was introduced in which the specimen is sonicated in the following agents to achieve proper cleaning: alconox, acetone, methanol, ethanol, and freon. Although this constitutes a longer process, the savings in SEM time is substantial.

ELECTRON MICROPROBE ANALYSIS

R. J. Bacon

In the SEM area emphasis is placed on microstructural characterization, with microanalytical techniques playing a secondary role; in the electron microprobe area, the emphasis is reversed. A strong interaction between SEM and microprobe enables scientists to achieve optimum results from microstructural and microanalytical techniques. A summary of EPMA support is given in Table 2.

TABLE 2
SUMMARY OF EPMA SUPPORT

Samples run	550
Micrographs taken	1,120
X-rays taken	18,000 - 20,000

The electron microprobe is not used extensively for micrographs but rather for x-ray spectra using Energy Dispersive Spectrometry (EDS) and x-ray counts using Wavelength Dispersive Spectrometry (WDS) with tuned crystals. The use of backscattered electron imaging aids in the final quantitative analysis, especially in samples containing alloying elements having large differences in atomic numbers [for example, Ti (at. 22) and Mo (at. 42)].

Many procedures have been established for collecting data rapidly and achieving quantitative results. The benefits of rapid data collection are as follows:

1. Beam regulation - Although the beam is stable for a certain period, drift eventually becomes a problem. When standards plus thirty or more points on the sample are run, beam drifting begins and quantitative numbers drift as well.
2. Extended filament life - In order to preserve the life of the filament, it must be kept on no longer than necessary for collection of data from standards and the sample.
3. Reduced sample contamination - Contamination must be kept to a minimum in order to avoid creation of an artifact.
4. Increased reproducibility of x-ray data.

The step following collection of x-ray data (either digital counts from WDS or spectra stored on disc from EDS) involves processing the data for quantitative weight and atomic percent for each element in the sample. Different procedures are required for achieving quantitative results using WDS and EDS. Since WDS is a digital count and EDS a spectrum display, different computer programs must be used for processing data from these two techniques.

The procedure for collecting WDS data is as follows:

1. Set condenser lens to desired specimen and aperture current.
2. Set beam regulator to ON and go through beam-regulating procedure.
3. Check aperture current to assure stability of the beam current.
4. Run standards for element peak counts and background counts.

5. Run sample and record element peak counts for a pre-set counting time period.
6. After analyzing the sample, rerun the standards, as in step 4, checking instabilities in beam current or drift in x-ray spectrometers.

The procedure for processing WDS data is as follows.

1. Use the AFWAL Materials Laboratory program called MAGIC. This program is straightforward, and the number of entries which must be punched into the program each time is kept to a minimum.
2. List accelerating voltage, elements in the sample along with K, L, and M lines and λ_B , the number of standards, the element for which the standard will be used, and the percentage of the element present in the standard (for example, for standard Ti-6Al-4V the percent Al is 6, percent V is 4, and percent Ti is 90). In this manner, one standard can be used for three elements or for any one of the three elements.
3. Enter the peak and background counts for standards and the counting time.
4. Take the peak and background counts from the sample, and take the counting time.
5. Once Steps 1 - 4 have been accomplished, put peak counts into the computer program for each element; the computer will print out the quantitative data.

With the purchase of new WDS crystals and detectors, detection of light elements was possible. The results previously were obtained by analyzing the other elements in the sample and calculating the difference

between that total and 100%. Boron, carbon, nitrogen, oxygen, and fluorine could be detected; but detection of such light elements is sensitive to sample preparation, and detection of trace amounts is not possible.

The procedure for collecting EDS spectra using the Kevex 7000 system for ZAF Standards is as follows:

1. Set up *9 f
2. Establish accelerating voltage
3. Make element list
4. Run standards for preset time
 - a. Read spectrum
 - b. Analyze background
 - c. Subtract background
 - d. Request results
 - e. Enter element
 - f. Request no quantitative results
5. SAVE spectrum on disc
 - a. Enter unit 0
 - b. Enter general comments
 - c. Enter spectrum ID
 - d. Enter elements to be included
 - e. Enter standard "yes"
 - f. Enter concentrations for element weight percent

The procedure for collecting EDS spectrum, saving on Disc 1, and processing data by ZAF standards saved on Disc 0 in the above steps is as follows:

1. Set up element list
2. Run sample to collect x-rays from desired area for a pre-set time period
 - a. read spectrum
3. STORE spectrum on Disc 1
 - a. Enter Unit 1
 - b. Enter general comments

- c. Enter spectrum ID
- d. Enter elements to be included
- e. Enter standard "No"
4. Repeat above procedure for the number of spectra required for analysis, storing these on Disc 1 for future
5. Process data into weight percent and atomic percent totaling $100\% \pm 2\%$.

Automatic command files (ATO's) are provided to allow the user to perform command and analysis sequences automatically. This feature is particularly useful when command sequences must be repeated during the analysis of spectra obtained from specimens of similar composition. ATO's are set up by recording the commands involved in an analysis sequence. The following ATO program consists of 18 commands.

1. SET LA: Establishes the number of spectra to be analyzed. The maximum number of spectra which can be processed is 31.
2. SET ID: Enters the name (ID) for each spectrum to be analyzed from Position A to Position 31.
3. RON,nn: Records a named ATO file; RON must be followed by a comma and the name of the file being recorded.
4. RCL: Recalls spectrum and associated parameters from disc.
5. 99: Deletes all marker lines, painted regions, and overlays from video display.
6. ESC (Escape): Removes all spectrum escape peaks and restores escape-peak energies to parent energy peaks.
7. BKA: Performs automatic background analysis.
8. BKS: Removes analyzed background from spectrum.
9. RES: Obtains the results of synthesis; extracts and prints out net peak intensities.
10. ALL: Stores all elements in the element list when spectrum is stored.
11. ENTER: Continues analysis of synthesis active.
12. Y (YES): Yields quantitative results.

- 13a. ZAF (Quantitative correction methods for bulk analysis): Uses MAGIC V to correct for matrix effects. Z - atomic number, A - absorption, or F - fluorescence (requires reference standards of known composition).
- 13b. APP (Approximate): uses ZAF corrections via MAGIC V for standardless analysis.
14. ALL: Quantitatively analyzes all elements on the element list when the spectrum is saved.
15. 1: Enter the number adjacent to the standard to be used for ZAF calculations of known compositions.
16. SETP0: (Set position command): Enters the spectrum position which will be recalled first. SETP0 can be advanced, one position at a time, by using the "+" key.
17. LOOP: Causes the system to return to the first ATO command and repeat the analysis sequence up to 32 times, depending on SET LA and SET ID.
18. ROF (Record off): Terminates recording of automatic file.

After an ATO file has been established, ATO,nn is typed to execute a named ATO file and ATO is typed to execute an unnamed ATO file. Once an ATO file has been activated, it will perform the analysis sequence automatically for up to 32 spectra with a running time of ~ 2 hr. As each of the 32 spectra are recalled from Disc 1 and the analysis sequence of the ATO program is performed, the quantitative weight and atomic percents are printed out on computer paper to provide a permanent record of the data.

Until recently, peak overlap was a serious problem in analysis of EDX data. For example, overlap in the TiK_{β} and VK_{α} peaks increased the peak height. New programs have been written to improve the accuracy; peak (TiK_{β}) is subtracted from peak (VK_{α}) and the remaining peak (VK_{α}) is analyzed quantitatively.

METALLOGRAPHY, PHOTOGRAPHY, AND HEAT-TREATMENT LABORATORIES

E. Harper

Support efforts in the areas of the metallography, photography, and heat treatment are summarized in Table 3. Descriptions of the techniques developed and research efforts conducted are presented below.

TABLE 3
SUMMARY OF SUPPORT ACTIVITIES

	Metallography	Heat Treatment	Photography
Samples Prepared	3,489	1,072	
Photographs Taken	5,249		10,141
Slides Made			8,488
Prints Made			
4 × 5 prints (39,781)			
5 × 7 prints (219)			
8 × 10 prints (1,592)			41,572
Miscellaneous			2,516

New Equipment

Micricon Computer Controller

In the characterization of materials, complex heat treatments are frequently required. An example of a typical work order for heat treating 0.375-diam. tensile specimens follows: 7 TLP bond cycles at 2050°F for 12 hr. under high vacuum (maximum cool-down rate = 50°F per 15 min. down to 1325°F), followed by precipitation heat treatment of 1325°F for 8 hr., cool at 100°F/hr. maximum to 1150°F for 8 hr., and then furnace cool.

With the aid of the Micricon Computer Controller, the TLP bond cycle with precipitation heat treatment was carried out extremely accurately with only a 4-manhr. set-up time; 27 manhr. was required for the remainder of the heat treatment. Without the controller, ~236 manhr. would have

been required and, with the furnace under manual control, the operator could not have accurately controlled the heating and cooling rates.

New Techniques

The following new techniques were formulated in the Metallography Lab during this contractual effort.

Volume Sample-Preparation Method with Automet

Several 1½-in. mounted samples were submitted for preparation. With the common procedure, 8 hr. was required for preparation of six samples. The person submitting the samples was instructed in the use of the Automet and a procedure for his samples established. Six Ti-6Al-4V specimens were mounted in 1½-in. Epomet and placed in a special holder for the Automet, and the following procedure was followed:

<u>STEP</u>	<u>ABRASIVE</u>	<u>TIME</u> (min)	<u>PRESSURE</u> (lb)	<u>SPEED</u>	<u>LUBRICANT</u>
1	120-grit SiC	3	40	low	H ₂ O
2	240-grit SiC	3	50	low	H ₂ O
3	320-grit SiC	3	40	low	H ₂ O
4	400-grit SiC	3	40	low	H ₂ O
5	600-grit SiC	5	45	low	H ₂ O
6	6-μ Diamond paste	3	40	low	oil
7	0.05-μ Alumina slurry	1	30	low	oil

In the above procedure most of the variables can be controlled, e.g., flatness, pressure, speed, consumables used, and time. With this procedure sample-preparation time was reduced to 21 min. (as compared to 8 hr.) and the desired quality maintained.

Polishing Method for Unusual Contour-Shaped Specimens

Six Inconel fatigue samples having an unusual contour shape were submitted for polishing. A new polishing method was designed to provide

the desired finish. A part for the drill press was designed and fabricated to hold a 1-in. polishing head. A 10-lb. load was applied to the sample, while the sample was rotated by the operator. SiC grit papers and final polishing cloth were cut to fit on this polishing head. The sample was ground to a 600-grit SiC finish, intermediate polished on microcloth with 6- μ diamond paste, and final polished on microcloth with 1- μ diamond paste.

Chemical-Attack Polishing

An attack-polishing procedure was formulated for metals having large hardness differences in the phases of the metal matrix. The following procedure was formulated specifically for Ti with 40% addition of W:

1. Grind samples to a 600-grit SiC finish.
2. Intermediate polish on red felt cloth with 6- μ diamond paste.
3. Final polish on microcloth using 0.5- μ chromic oxide in a 2% solution of HF.

Several variations of this method were formulated for a variety of alloys exhibiting similar characteristics.

Volume-Sample Preparation of Ni-Base Superalloys

The following metallographic technique was developed for preparation of Ni-alloy samples:

STEPS

1. Section sample by means of diamond saw.
2. Encapsulate material in 1-in. mounts with Epomet molding compound.
3. Place six encapsulated specimens in the 1-in. Automet holder.
4. Place 8-in. 120-grit SiC disc on Automet; grind on high speed at \sim 50 psi with water lubrication. Section for 2 min. or until all samples are flat.

5. Grind sample 2 min. on 8-in. 180-, 240-, 320-, 400-, and 600-grit SiC discs at 50 psi, cleaning sample between stages of SiC grits to prevent contamination.
6. Place 8-in. nylon cloth on Automet; charge with 6- μ diamond paste; polish sample 2.5 min. at 50 psi with Metadi fluid lubrication on high speed.
7. Clean sample in ultrasonic cleaner in solution of methanol for 2 min.
8. Place 8-in. microcloth on Automet; charge with 0.5- μ chromic-oxide slurry; polish 2 min. on low speed and then 2 min. at 30 psi.
9. Repeat Step 7.
10. For a scratch-free surface, place sample in vibratory polisher on microcloth in a 0.05- μ Alumina slurry on high for 5 min.

Volume Sample Preparation of RST and LD Fibers

The following technique was developed for the preparation of Ti-alloy RST and LD fibers using the Automet polishing system:

STEPS

1. Mount sample in finely ground 1-in. Epomet mounts.
2. Place mounts in Automet 1-in. holder.
3. Grind sample for 2 min. (or until flat) on 8-in. 600-grit SiC disc at 40 psi on high speed.
4. Intermediate polish on 8-in. red felt cloth charged with 6- μ diamond paste and lubricate at 40 psi and high speed for 2.5 min.
5. Final polish on 8-in. microcloth charged with 0.5- μ chromic-oxide slurry at 20 psi on high speed for 1.5 min.

NOTE: Samples must be ultrasonically cleaned between stages of grinding and intermediate and final polishing to prevent contamination.

Electropolishing to Remove Residual Surface Stress

Ti-6246 threaded tensile specimens were submitted for preparation of the surface to a mirror-like and scratch-free condition. An electrolytic polishing method was to be used to remove residual surface stress (see Fig. 3). A curve on removal of residual surface stress in Ti-6246 was obtained from a paper by Paradee.⁶ The curve shows that removing 0.38 mm of material by electrolytic polishing renders the sample free of residual surface stress (see Fig. 4).

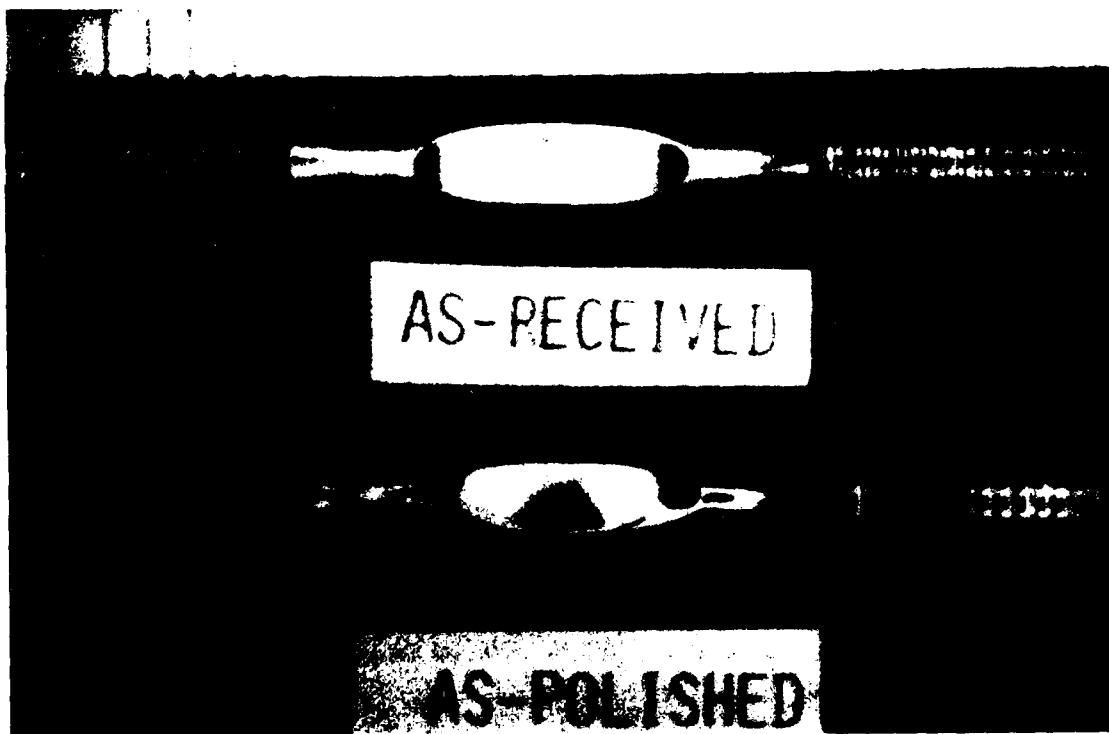


Figure 3. Short-Crack Fatigue Samples, As-Received and After Removal of 0.38 mm of Material by Electrolytic Polish.

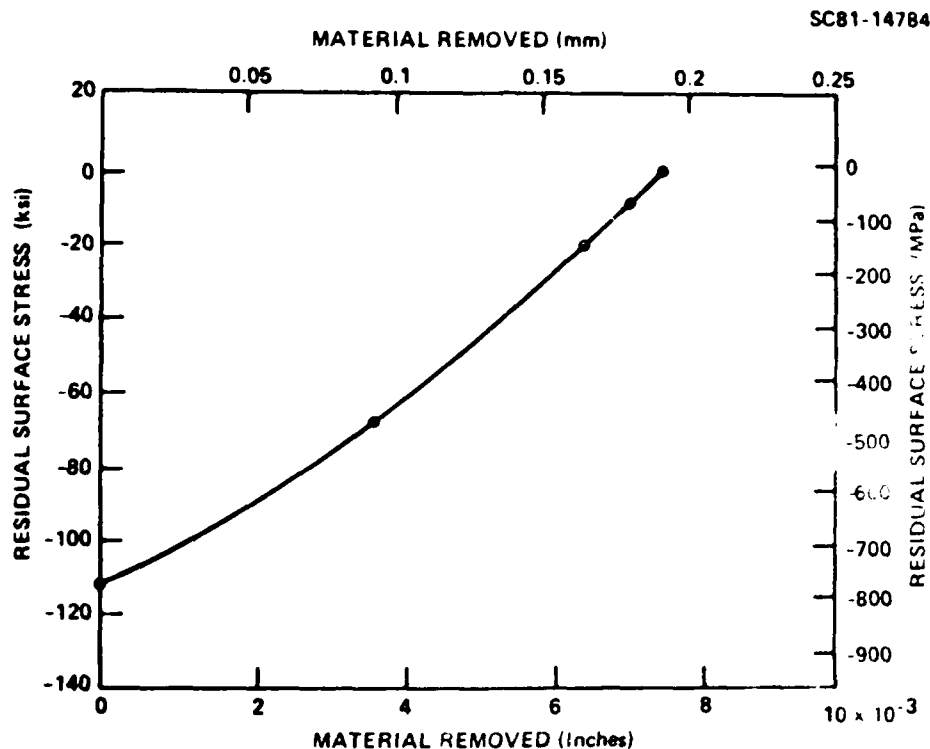


Figure 4. Residual Surface Stress Measured on Carefully Milled Ti-6246 Surface as Function of Depth of Material Removed by Polish (from Ref. 6).

Because of the odd shape of the sample, the following unique electrolytic polishing system was designed. An electrolytic polishing cell was made from a 100-ml Pyrex beaker placed in an insulated magnetic stirring bowl which contained 0.5 gal. of methanol. A Teflon-coated magnetic stirrer was placed in the Pyrex beaker which had been filled with 60 cc perchloric acid (60%), 590 cc methanol, and 350 cc butyl cellusolve. The threaded ends of the specimens were coated with Micro-stop lacquer to prevent the electrolyte solution from polishing the threads. Liquid nitrogen was poured into the methanol bath to maintain the temperature of the electrolyte at $-40^{\circ}\text{C} \pm 5^{\circ}\text{C}$. The rheostat on the magnetic stirrer was placed in the half-open position

to achieve medium agitation of the electrolyte. A stainless-steel cylinder-shaped cathode was placed in the electrolyte. An anode machined from stainless steel was used to hold the threaded specimens to be mounted on the shaft of a variable-speed stirring motor. The shaft was driven at 125 rpm, and the rotation was opposite to that of the agitation of the electrolyte. The specimens were electrolytically polished for 20 min. at 6.0 A. The electrolyte was removed from a 6.35-mm specimen was removed at a rate of 0.002 mm per min. The samples produced had a surface free of scratches with scratch- and stress-free surfaces.

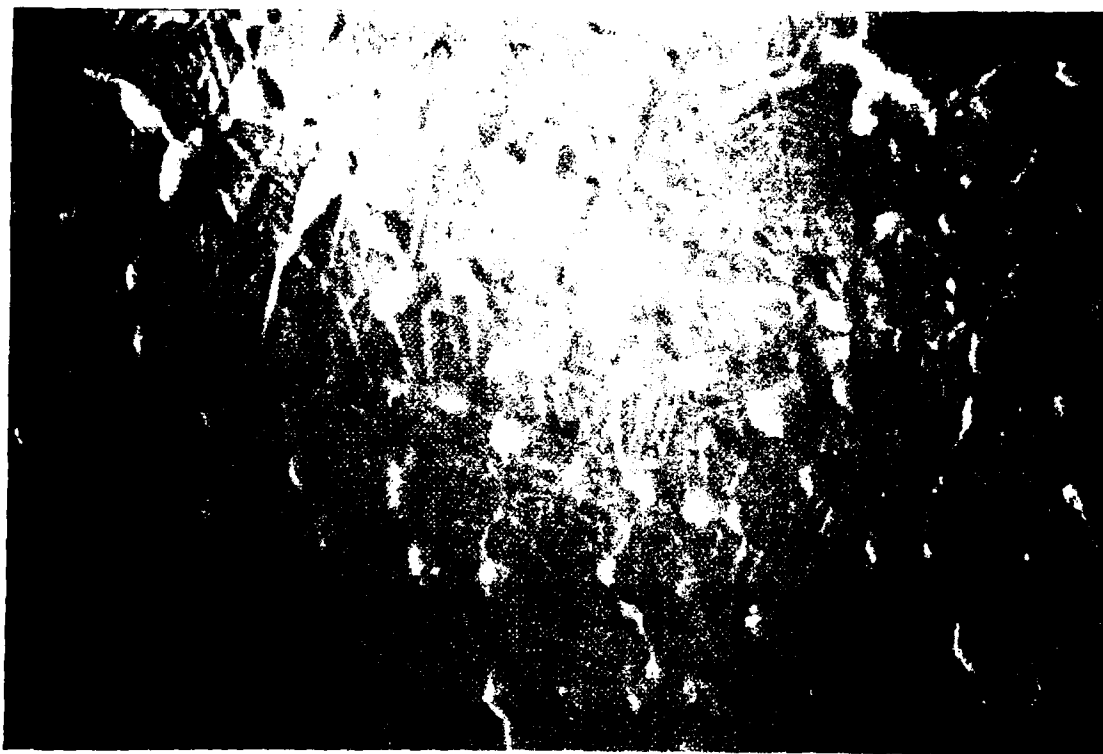


Figure 5. Micrograph Revealing Fine Microstructure of Ti-6246 After Electrolytic Polishing. Magnification 60x under polarized light.

Polishing Machined Line to Remove Surface Damage on Fatigue Samples

An IN-718 compact-tension specimen with a machined line required polishing to a mirror-like finish to remove the surface of fatigue crack growth during testing. Because of the small thickness of the line,

manual polishing methods were impractical. Therefore, the following electrolytic polishing system was developed.

A polishing cell made from a 1000-ml Pyrex beaker was placed in an insulated magnetic stirring bowl containing 0.5 gal. methanol. A Teflon-coated stirrer was placed in the Pyrex beaker which had been filled with 60 cc perchloric acid (60%), 590 cc methanol, and 350 cc butyl cellosolve. Parts of the sample which were to remain unpolished were coated with Micro-stop lacquer.

Liquid nitrogen was then poured into the methanol bath to maintain electrolytic temperatures at $-40^{\circ}\text{C} \pm 5^{\circ}\text{C}$. The rheostat on the magnetic stirrer was placed in the half-open position to achieve medium agitation. A cathode was made from a flat piece of stainless steel and placed in the beaker. A fixture to hold the specimen or anode was also made from stainless steel. The specimen was electrolytically polished for 15 min. at 50 VDC-3 amps which produced a mirror finish.

Electropolishing Technique for Large Ti-10-2-3 Samples

Ti-10-2-3 samples which had been subjected to various heat treatments were submitted for preparation. Electropolishing was chosen because of the difficulty which had been encountered in attempts to reveal the fine details in the matrix by mechanical polishing. The following method was formulated and applied.

A polishing cell made from a 1000-ml Pyrex beaker was placed in an insulated magnetic stirring bowl containing 0.5 gal. methanol. A Teflon-coated magnetic stirrer was placed in the Pyrex beaker which had been filled with 60 cc perchloric acid (60%), 590 cc methanol, and 350 cc butyl cellosolve.

Liquid nitrogen was poured into the methanol bath to maintain the electrolyte temperature at $40^{\circ}\text{C} \pm 5^{\circ}\text{C}$. The rheostat was placed in the half-open position to achieve medium agitation. A large flat piece of Ti-10-2-3 was used as a cathode. A commercially pure Ti rod was welded

onto the anode to permit positioning in the electrolyte. Parts of the specimen not requiring polishing were coated with Micro-Stop lacquer. Samples were electrolytically polished for 12 min. at 52 VDC, 4 amp; and excellent results were achieved.

Special Lighting Techniques to Enhance Macro-grain Contrast

Large polished and macro-etched Ti-10-2-3 samples were macrophotographed at approximately a 1:1 ratio to reveal the differences in grain contrast and other fine details. The MP-1 camera was used in conjunction with special lighting techniques, and several high-quality photographs were obtained (see Fig. 6).

Evaluation of Automatic Polishing and Grinding Systems

E. Harper visited the facility of Leco Corporation for a demonstration of the P-100 automatic grinder and P-200 automatic polisher. Twelve mounted Ti powder-metal samples from the AFWAL Materials Laboratory were used for the demonstration. These samples were ground and polished in 10 min. of machine time. Although the machine performed well, it had limitations relative to the number of specimens which could be accommodated, the pressure limit of 150 psi on grinding, and the very high probability of directional polish which can be attributed to the design of the machine.

E. Harper also visited the facility of Buehler, Ltd., for a demonstration of the new Maximet polisher and grinder. Twenty-four mounted Ti powder-metal samples from the AFWAL Materials Laboratory were used for the demonstration. These samples were ground in only 5 min. of machine time. The strong points of this machine are:

1. The powder diamond lapping system uses no polishing cloths and a less expensive diamond compound.
2. Grinding and polishing can be implemented on the same machine.
3. Twenty-four samples can be ground and polished in only 5 min. of machine time (as compared to 2-3 hr./sample for manual mechanical polish).



(a)

(b)



(c)

Figure 6. (a) Ti-10V-1Fe-3Al Microstructure Revealing Deformed Grains in Matrix (30% Reduction) at 925°C. Magnification 4×
 (b) Recrystallized Grain Structure Superimposed with Image of Original Deformed Grain Structure in Annealed and Quenched Specimen. Magnification 4×
 (c) Recrystallized Grain in Annealed and Quenched Specimens After Removal of Deformed-Grain "Ghost" Boundaries. Magnification 4×.

4. Samples up to 11-in. section can be ground and polished unmounted.
5. Savings in consumables alone would pay for the machine in approximately 1 yr.

Of the two systems, the Buehler machine was determined to better fit the needs of the laboratory, and the recommendation was submitted to the contract monitor.

SPECIAL PROJECT

A. Jackson

Pendant Drop Melt Extraction (PDME) Ti Ribbon

To characterize the microstructures of rapidly solidified alloys, a PDME apparatus was constructed by SRL personnel. This capability allows preparation of RST ribbon of Al and Ti alloys under various cooling rate conditions.

The apparatus consists of a 200-mm- (8-in.-) diam. Cu wheel driven by a variable-speed motor (500-10,000 rpm) through a belt drive and high-vacuum feed-through. The rod to be melted is lowered by a screw drive to a position immediately above the wheel, which is oriented with the rotational axis perpendicular to the rod. A hot filament for providing electrons is located around the tip of the rod, and a negative accelerating voltage of up to 2 kV at 1.5 ADC is applied to the filament. Power of 3 kW (max) is sufficient to liquify a Ti rod of less than 13-in. (1 1/2-in.) diam.

The design of the apparatus is based on published descriptions of PDME systems built by Battelle and descriptions provided by Battelle personnel during visits to their Columbus laboratories. The SRL apparatus is simpler in design since it does not include a water cooled wheel, uses a belt drive, and incorporates a unique filament assembly which reduces the power required to melt material. The filament assembly consists of a W wire formed into a partial circle to surround the material to be melted. An electron reflector is provided adjacent to the filament to increase the beam current to the material. When the

reflector was used, a significant reduction in the power required to melt material was noted. The "V"-shaped reflector is mounted to one of the filament terminals, with the "V" opening being toward the filament (Fig. 7). Various reflector geometries are possible, depending on the filament size. Simple "V" shapes have been used as well as curved shapes which approximate the filament geometry. The vacuum system used is a 457-mm- (18-in.-) diam. glass bell jar diffusion pumped to $\sim 7 \times 10^{-4}$ Pa (5×10^{-6} Torr).

The power supply employed for the filament is a standard 12-V auto battery. Accelerating voltage is provided by a specially designed variable DC voltage circuit (full-wave rectifying with ballast for current surges). Commercial power supplies with short-circuit (large current limiter) features to protect the circuit against arcing between the filament and ground were unavailable. The design used does not fully protect against high-speed arcing, but slow changes in current are handled by the ballast lamps.



Figure 7. Schematic Diagram Showing Filament Assembly Used in PDME Apparatus. (a) Side View, (b) Three-Quarter View.

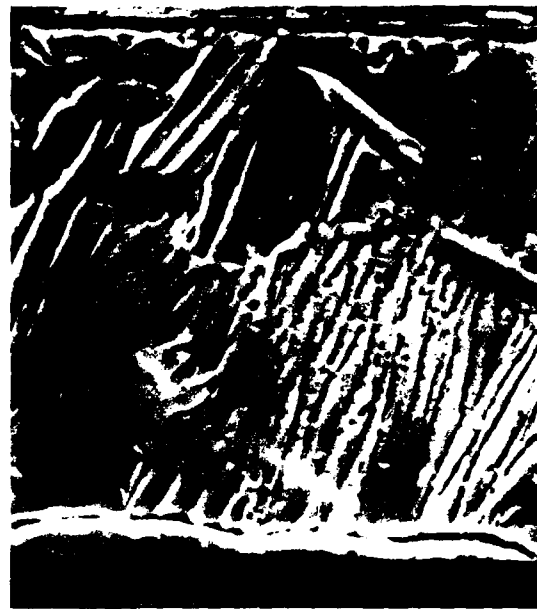
Ribbon was made from CP Ti rod using various wheel-rotational speeds in order to observe the effect on the microstructure. Micrographs of ribbon cross sections for various speeds are shown in Fig. 8(a) - (f). As expected, the faster the wheel speed, the finer the microstructure.

Tangential velocity as a function of rotational speed is plotted in Fig. 9. The tangential velocity is a measure of the cooling rate since the liquid solidifies while in contact with the wheel, at low speeds, and experiences a large temperature drop at the higher speeds, where solidification must be completed after the material leaves the wheel. Since the time during which the material is in contact with the wheel decreases with increasing speed and since the contact area is assumed to be constant, the cooling rate is proportional to the wheel speed, the exact dependence being alloy dependent.

Experimentally the measurable quantities are the ribbon thickness and width. Through heat-flow considerations the thickness has been shown to be proportional to the inverse square root of the cooling rate. Thus, measurement of thickness as a function of speed was expected to yield a curve which could be used to relate wheel speed to cooling rate. The plot of thickness as a function of wheel speed (Fig. 10), however, has a significant amount of scatter, which is interpreted to arise from transients in the solidification process. As a result, the specimens used did not represent an acceptable sampling of the ribbon. Hence, additional ribbon must be generated which represents stable solidification.



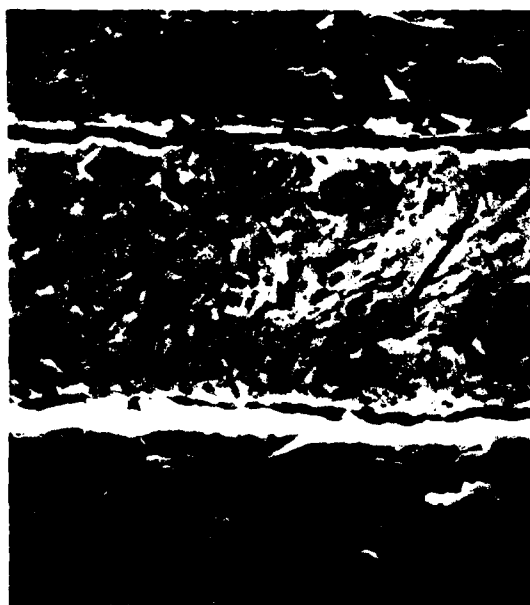
(a)



(b)



(c)



(d)

Figure 8. SEM Micrographs of CP Ti PDME Ribbon Produced at Various Rotational Speeds. (a) 1400 RPM, (b) 2000 RPM, (c) 2100 RPM, (d) 2850 RPM, (e) 3000 RPM, (f) 3600 RPM.



(e)



(f)

Figure 8. (Continued)

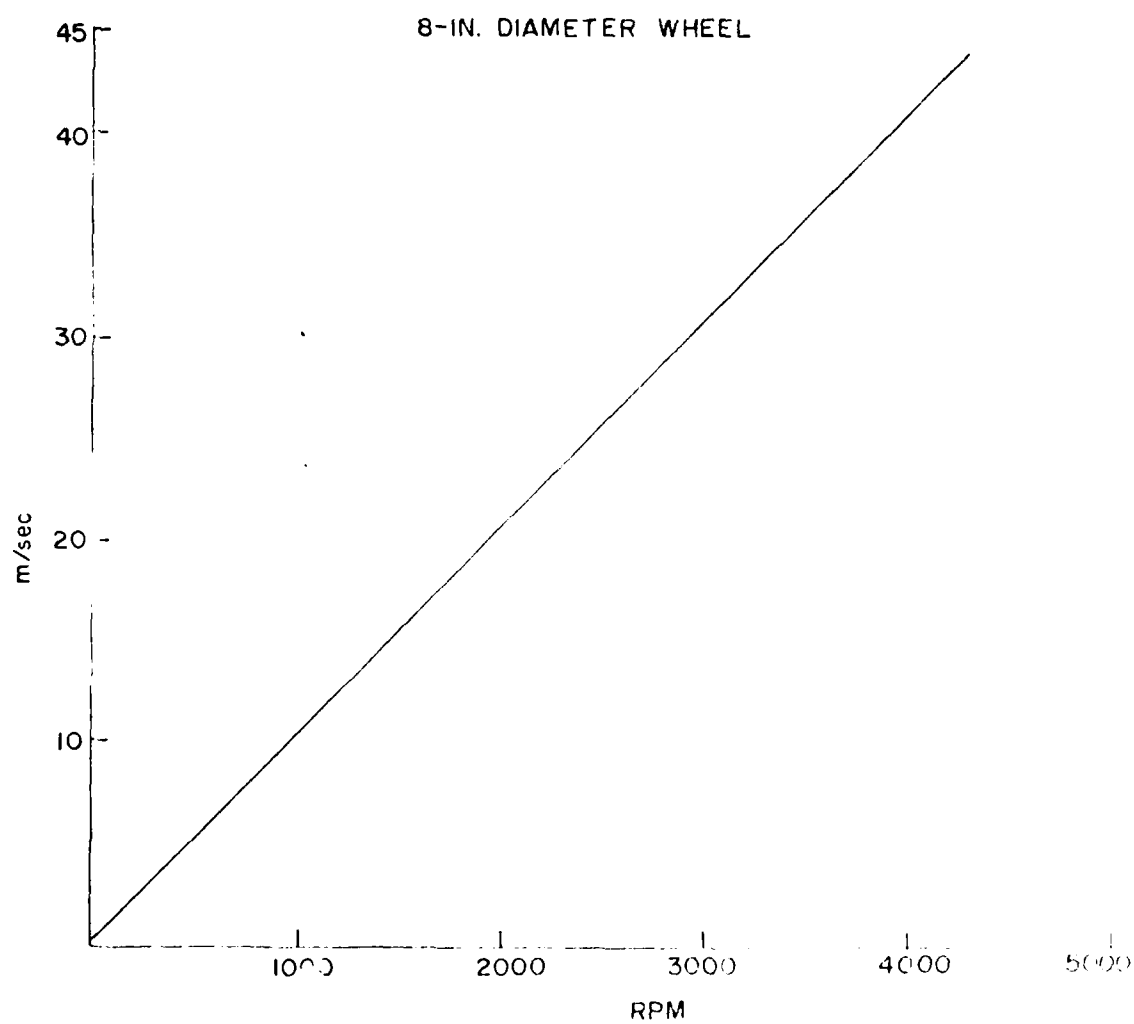


Figure 9. Plot of Wheel Tangential Velocity as Function of Rotational Speed for PDME Apparatus.

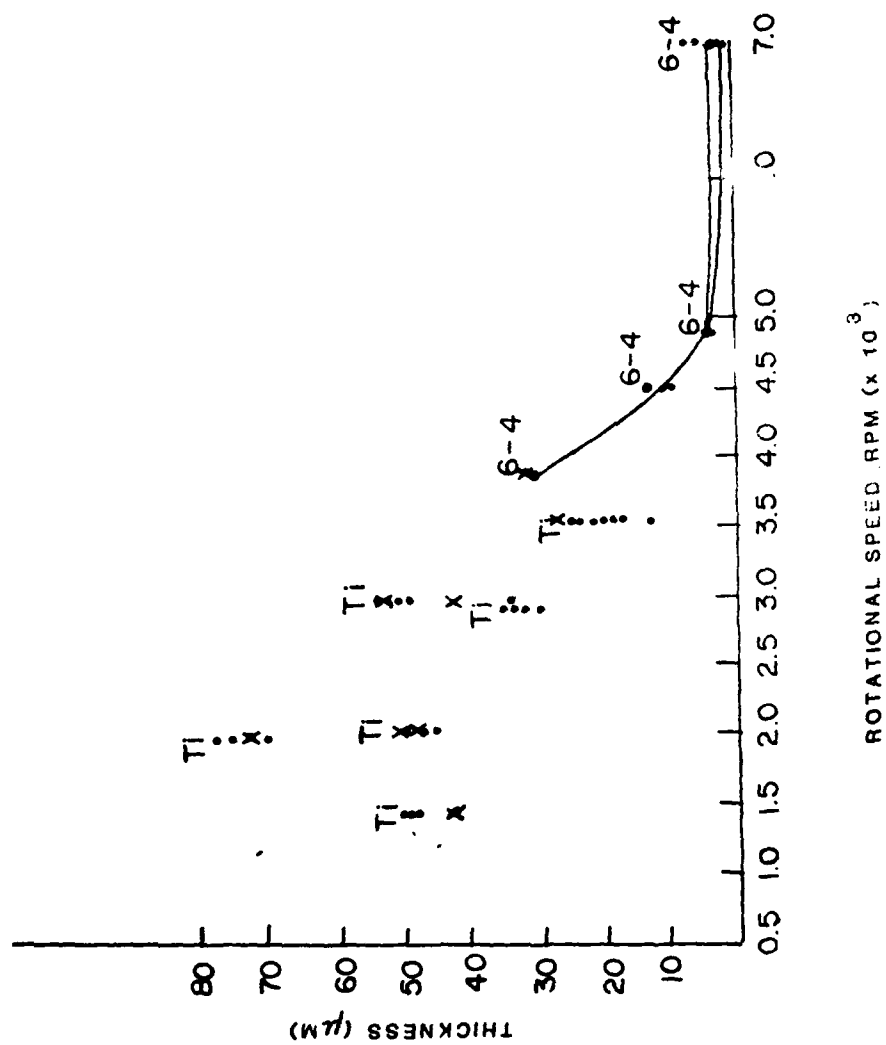


Figure 10. Ribbon-Thickness data plotted as function of rotational speed. Scatter in data arose from sampling of ribbon when maximum reduction was reached.

Types of Cooling in Ribbon Produced by Rapid-Solidification Technology (RST)

The cases for Ideal (infinite heat transfer) and for Newtonian (low heat transfer) cooling in RST are considered by Ruhl⁷ in terms of a number of experimental variables.

An important number referred to by Ruhl and many other authors who conducted subsequent studies is the Nusselt number

$$Nu = hd/k_s,$$

where

h = thermal transfer coefficient ($\text{cal}/\text{cm}^2\text{-sec.}-^\circ\text{C}$),

d = splat thickness (cm),

k_s = thermal conductivity ($\text{cal}/\text{cm-}^\circ\text{C-sec.}$).

Ruhl shows that for $Nu < 0.015$, cooling is Newtonian; while for $Nu > 0$, cooling is Ideal. He provides a table of Nu values for various substrates, which indicates that Newtonian and intermediate cooling are dominant for this metal.

In Table 4 values of Nu for Ti (Cu substrate assumed) are given. The numbers indicate that for $d < 10^{-4}$ cm and $h < 1$ $\text{cal}/\text{cm}^2\text{-}^\circ\text{C-sec.}$, Newtonian cooling can be expected to dominate. For $h > 1$ and $d > 10^{-4}$, intermediate and Ideal cooling dominate. For splat or PDME processes, the thickness range is frequently 10μ to $100 - 200 \mu$ and h is greater than 1, since solidification occurs in a high-conductivity substrate. Thus, for Ti, intermediate and Ideal cooling are expected to dominate.

TABLE 4
NUSSELT NUMBERS FOR VARIOUS VALUES OF
HEAT-TRANSFER COEFFICIENT, h , and THICKNESS, d

$h =$		1000	100	10	1
(μ)	d (cm)				
(1)	10^{-4}	3.1	0.31	0.031	0.0031
(10)	10^{-3}	31	3.1	0.31	0.031
(100)	10^{-2}	310	31	3.1	0.31

$[K_s]_{T_i} = 0.032 \text{ cal/cm}^2\text{-}^\circ\text{C-sec}]$

TABLE 5
DIMENSIONLESS TIME AS A FUNCTION OF h AND t FOR T_i AND A_1

		T_i				
N	h/t	10^{-6}	10^{-5}	10^{-4}	10^{-3}	10^{-2}
	1	5.6×10^{-5}	5.6×10^{-4}	5.6×10^{-3}	5.6×10^{-2}	5.6×10^{-1}
	10	5.6×10^{-3}	5.6×10^{-2}	5.6×10^{-1}	5.6×1	
I	100	5.6×10^{-1}	5.6×1	5.6×10	5.6×10^2	5.6×10^3

		A_1				
N		10^{-6}	10^{-5}	10^{-4}	10^{-3}	10^{-2}
	1	3.25×10^{-6}	3.25×10^{-5}	3.25×10^{-4}	3.25×10^{-3}	3.25×10^{-2}
	10	3.25×10^{-4}	3.25×10^{-3}	3.25×10^{-2}	3.25×10^{-1}	3.25×1
I	100	3.25×10^{-2}	3.25×10^{-1}	3.25×10	3.25×10^1	3.25×10^2

N = Newtonian, I = Ideal

An alternative approach to considering the effect of various parameters on solidification is the use of a reduced solidification time or dimensionless time, in the manner of Katgerman,⁸

$$\tau = h^2 a t / k_s^2,$$

where h = heat-transfer coefficient,

$$a = k_s / \rho C_p,$$

k_s = thermal conductivity,

ρ = density,

C_p = specific heat,

t = real time.

In Table 5, τ for various values of h and t for Ti and Al is given. The difference in τ between the two metals is about one order of magnitude, Al possessing the shorter times. Hence, from the tables, 1) Al is expected to solidify in shorter times and, thus, should be easier to solidify rapidly than Ti, and 2) the thickness of ribbon should be less sensitive to operating parameters than in the case of Ti.

In the PDME method and in splat cooling, high thermal transfer is being used experimentally, which means large values of h . The assumption has been that as much heat as quickly as possible must be extracted by impinging the melt onto a high-thermal-conductivity substrate such as Cu. Hence, conditions are established to approach Ideal cooling; but frequently reported cooling rates are based on Newtonian cooling estimates. Katgerman predicts that the larger the dimensionless time, the closer to Ideal the cooling and the lower the cooling rate. For short times, the rate is a constant. This is in direct opposition to Ruhl's work which shows ideal cooling to be associated with short solidification times and high cooling rates. The contradiction can be resolved if Katgerman's Fig. 2 is redrawn with the intermediate cooling curve above the Ideal and Newtonian lines (See Fig. 11). In this interpretation for long solidification times, Newtonian cooling at a constant rate dominates; while for very short times, Ideal cooling dominates, with the rate being proportional to $1/\sqrt{t}$. Experimentally this interpretation seems to fit the observations.

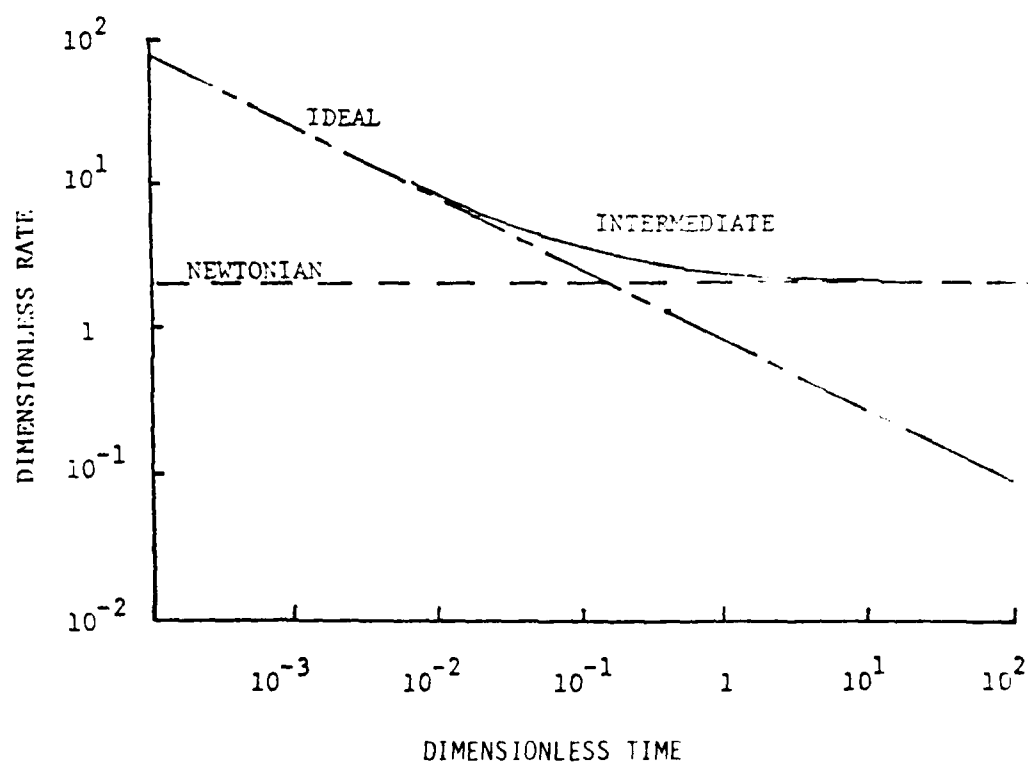


Figure 11. Plot of Cooling Rate vs. Time for Dimensionless Variables Used by Katgerman (redrawn Fig. 2 from Ref. 8).

Applying this interpretation to the values in Table 2, it is apparent that Al has a higher cooling rate than Ti, assuming the same conditions for the two alloys. Thus, if high cooling rates for Ti are desired (about the same as those for Al), then solidification times for Ti must be shorter by about a factor of 10, making RST Ti more sensitive to the operating conditions prevailing in the RST method.

In any case the use of high-thermal-conductivity substrates for Ti alloys will increase the solidification time and lead to more level structures; however, other effects then become important, such as viscosity of the melt, substrate temperature, speed of the substrate, and (for PDME) mass transfer from the melt to the ribbon.

For the case of Ideal cooling, Katgerman has given the velocity of the solidification front as

$$V_s = \gamma \sqrt{\pi/t}.$$

where γ is found numerically from

$$\gamma \exp(\gamma^2) \operatorname{erf}(\gamma) = (T_M - T_0) C_p / H \sqrt{\pi},$$

T_M = melt temperature,

T_0 = substrate temperature,

C_p = specific heat of the melt,

H = heat of fusion/unit mass of melt.

As V_s increases and time decreases, the Ideal cooling condition is approached, but momentum effects in the solid/liquid interface may alter the results which can be expected when no momentum layer is assumed, i.e., when there is no drag on the liquid as it moves away from the source. These momentum effects relate to the expected thickness of the ribbon. The thickness of the ribbon with no momentum layer is given by

$$d = V_s t,$$

while that of the ribbon with a momentum layer and Ideal cooling is given by

$$d = V_s t + C\sqrt{vt},$$

where C = constant between 1 and 10

v = kinetic viscosity = viscosity/density.

On the basis of the foregoing considerations, the following conclusions can be drawn:

1. For Ti alloys, assumption of Newtonian cooling is not justifiable. The more complex Ideal cooling is the more correct assumption from which to start when making estimates.
2. Ti is more susceptible to choice of experimental operating parameters than Al.
3. The choice of substrate is not critical for Ti with respect to heat transfer.
4. Other parameters and variables are more important for Ti than for Al. Hence, the choice of operating conditions may be critical in terms of the structures produced.

Calculations of Weight Percent of Constituents in Ge Precipitate in Alloy with 7.5 Weight Percent Ge Aged for 40 hr. at 535°C.

Procedure

The weight percent Ge and Ti contained in the precipitates observed can be calculated in two ways. The first method is based upon that of Cliff-Lorimer; the second is based upon that of Zaluzec. Both are explained in Analytical Electron Microscopy,⁹ in terms of a single-phase material. Physically, the problem at hand is determining the composition of a precipitate embedded in a matrix. X-ray counts collected from this region contain contributions from both precipitate and matrix. Thus, the methods applied to a single-phase alloy must be modified to take into account the contributions of both matrix and precipitate and permit accurate separation of each contribution. The

bases for the calculation are that (1) local homogeneity is present in the matrix surrounding the precipitate, and (2) at least one element appears in the matrix which does not appear in the precipitate. The procedure is to find concentration ratios for the elements in the matrix using an appropriate method and subsequently employing these ratios to determine the matrix contribution to the amounts measured from a region containing a precipitate.

Method 1

The concentration ratio is given by

$$\frac{C_A}{C_{Ref}} = K_{ARef} \frac{I_A}{I_{Ref}},$$

where $K_{ARef} = \frac{K_A}{K_{Ref}},$

C_A = concentration of element A,

C_{Ref} = concentration of element used as reference,

I_A = integrated intensity of A,

I_{Ref} = integrated intensity of reference element,

K_A = Cliff-Lorimer factor for A,

K_{Ref} = Cliff-Lorimer factor for reference element.

For the case at hand, the elements are Al, Ge, Sn, and Ti, where Ti serves as the reference element. The ratios for the matrix are given by

$$\frac{C_{Al}}{C_{Ti}} = \frac{K_{Al}}{K_{Ti}} \frac{I_{Al}}{I_{Ti}},$$

$$\frac{C_{Ge}}{C_{Ti}} = \frac{K_{Ge}}{K_{Ti}} \frac{I_{Ge}}{I_{Ti}},$$

$$\frac{C_{Sn}}{C_{Ti}} = \frac{K_{Sn}}{K_{Ti}} \frac{I_{Sn}}{I_{Ti}}.$$

The K-factors for these elements are known, and the integrated intensities are obtainable experimentally. Hence, experimental ratios can be found, and from these the weight percent of each element, with the assumption that the sum of concentrations is 1.00, can be determined.

Counts obtained from the region containing the precipitate include both matrix and precipitate. If the matrix surrounding the precipitate is uniform, the ratio of elements in a precipitate-free region (Region 1) and that in the precipitate-containing region (Region 2) will be the same except for the contribution by the precipitate (Fig. 12). If one element appears in the matrix but not in the precipitate, then the counts from this element can be used as the starting point for calculation of the matrix contribution in Region 2 (Table 6).

TABLE 6
CONTRIBUTIONS TO MEASURED INTENSITY

	Ti	Al	Sn	Ge
Matrix	yes	yes	yes	yes
Precipitate	yes	no	no	yes

The concentration ratios for Region 2 are

$$\frac{C_{Al}'}{C_{Ti}'} = \frac{K_{Al}}{K_{Ti}} \frac{I_{Al}'}{I_{Ti}'},$$

$$\frac{C_{Ge}'}{C_{Ti}'} = \frac{K_{Ge}}{K_{Al}} \frac{I_{Ge}'}{I_{Ti}'},$$

$$\frac{C_{Sn}'}{C_{Ti}'} = \frac{K_{Sn}}{K_{Al}} \frac{I_{Sn}'}{I_{Ti}'}.$$

For this case, the starting assumption is that no Al is present in the precipitate.

Since concentration ratios for Al are equal in both regions, Ti from the matrix in Region 2 is

$$I_{Ti}' = \frac{K_{Al}}{K_{Ti}} I_{Al}' \frac{C_{Al}}{C_{Ti}},$$

and the contribution of Ge from the matrix in Region 2 is

$$I'_{\text{Ge}} = \frac{C'_{\text{Ge}}}{C'_{\text{Ti}}} \frac{K_{\text{Ti}}}{K_{\text{Ge}}} I'_{\text{Ti}}.$$

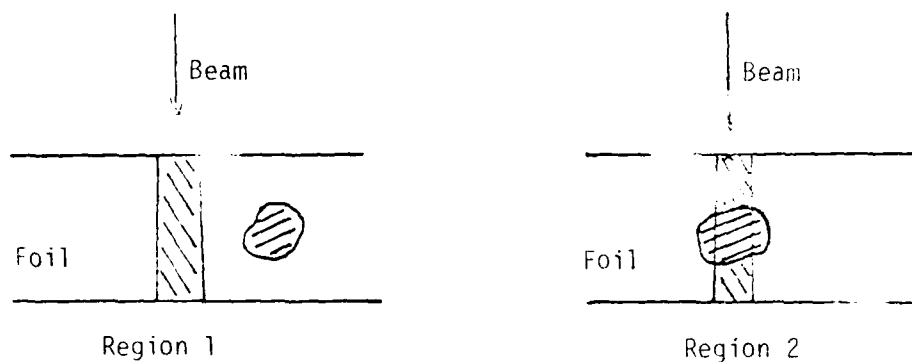


Figure 1. Regions of Foil With Precipitate (1) and Without Precipitate (2).

The difference between the measured intensity from Region 2 and the calculated intensities due to the matrix is given by

$$I(\text{Ti}) = I''_{\text{Ti}} - I'_{\text{Ti}},$$

$$I(\text{Ge}) = I''_{\text{Ge}} - I'_{\text{Ge}},$$

where I''_{Ti} and I''_{Ge} are the measured intensities from Region 2. Finally, the concentration ratio for the precipitate is written as

$$\frac{C_{\text{Ge}}}{C_{\text{Ti}}_{\text{ppt}}} = \frac{K_{\text{Ge}}}{K_{\text{Ti}}} \frac{I(\text{Ge})}{I(\text{Ti})},$$

from which the weight percents are calculated on the assumption that the sum of the two elements is 100%.

Method 2

A simpler derivation of net counts is as follows. The Ti matrix contribution from Region 2 is given by

$$I'_{Ti} = \frac{I'_{Al}}{I_{Al}} I_{Ti} ,$$

while the Ge matrix contribution from this region is

$$I'_{Ge} = \frac{I_{Ge}}{I_{Ti}} I'_{Ti} .$$

Thus, the net counts from the precipitate are given as the difference

$$I_N(Ti) = I''_{Ti} - I'_{Ti} ,$$

$$I_N(Ge) = I''_{Ge} - I'_{Ge} .$$

The concentration-ratio calculation can be carried out by use of the Cliff-Lorimer ratio, as given above:

$$\frac{C_{Ge}}{C_{Ti}} = \frac{K_{Ge}}{K_{Ti}} \frac{I(Ge)}{I(Ti)} ,$$

or by use of the Zaluzec method, in which the same principles hold through the net-count calculation. Concentration ratios, however, are found by using

$$\frac{C_{Ge}}{C_{Ti}} = \epsilon \kappa \frac{I_N(Ge)}{I_N(Ti)} ,$$

where $\epsilon = \epsilon_{Ti}/\epsilon_{Ge}$ = ratio of detector efficiencies (k lines) and $\kappa = \kappa_{Ti}/\kappa_{Ge}$ = ratio of x-ray generation constants, known for a given microscope beam energy (100 keV).

Results

Data from 19 precipitates were taken (Fig. 13), and the Ti and Ge concentrations in the precipitate were found using Methods 1 and 2; the results are given in Tables 7 and 8. The average weight percents using the Cliff-Lorimer method are 61.8 ± 7.9 w/o Ti and 38.2 ± 7.9 w/o Ge and, for Zaluzec, 58.6 ± 6.4 w/o Ti and 41.5 ± 6.4 w/o Ge.

From electron diffraction patterns, the precipitate is identified as Ti_5Ge_3 , which contains 52.4 w/o Ti and 47.6 w/o Ge. Thus, neither calculation yields satisfactory concentrations, although Zaluzec's method gives the closest agreement.

Absorption Considerations

In STEM, composition analysis calculations are made on the assumption that no absorption, atomic number or fluorescence corrections are necessary because the foil is sufficiently thin to reduce the x-ray excitation volume to a column the diameter of the beam.

If foil conditions depart from this assumption, then additional corrections must be made. Usually the largest correction is absorption, and the method for applying this correction has been developed (see Analytical Electron Microscopy,⁹ p. 152).

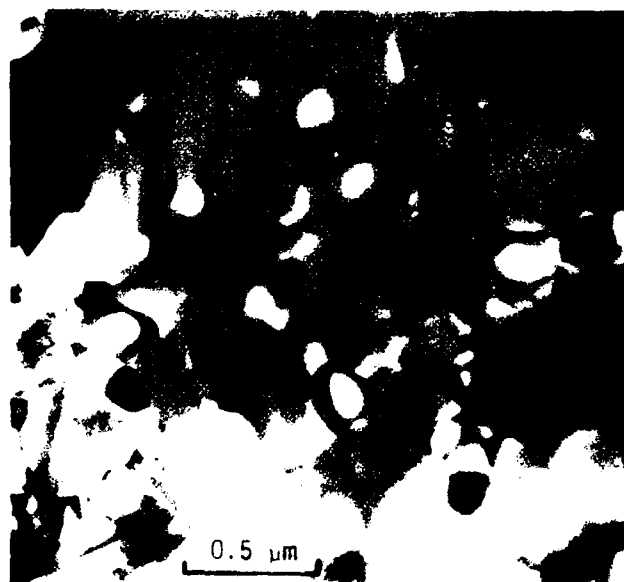


Figure 13. STEM Micrograph of Area From Which Intensity Measurements Listed in Table 6 Were Made.

TABLE 7
RESULTS OF CALCULATIONS OF Ti AND Ge PRESENT
IN PRECIPITATES USING CLIFF-LORIMER METHOD
(SPECIMEN AGED 40 HR AT 535°C)

No.	Ti	Ge	w/o	
1.	53.6	46.4		
2.	61.3	38.7		
3.	74.9	25.1	Ti ₅ Ge ₃	Ti 54
4.	62.6	37.4		Ge 46
5.	79.2	20.8		
6.	58.2	41.8	Ti ₃ Ge	Ti 67
7.	60.5	39.5		Ge 33
8.	70.2	29.8		
9.	63.9	36.1		
10.	60.2	39.9		
11.	67.2	32.8		
12.	43.0	57.0		
13.	55.7	44.3		
14.	63.9	36.1		
15.	61.0	39.0		
16.	65.0	35.0		
17.	55.7	44.3		
18.	58.2	41.8		
19.	60.3	39.7		
Avg. =				
σ =				
	61.8	38.2		
	± 7.9	± 7.9		

TABLE 8
RESULTS OF CALCULATIONS OF Ti AND Ge
PRESENT IN PRECIPITATE USING ZALUZEC METHOD

No.	Ti	Ge
1	57.1	42.9
2	57.5	42.5
3	67.3	32.7
4	62.4	37.6
5	58.9	41.2
6	66.4	33.6
7	40.6	59.4
8	54.8	45.2
9	61.2	38.9
10	60.3	39.7
11	62.7	37.3
12	55.1	44.9
13	57.3	42.8
14	58.3	41.7
Avg. =		
σ =		
	58.6	41.5
	± 6.4	± 6.4

Values of ε'κ from Analytical Electron Microscopy⁹

In Zaluzec's method, the concentration ratio is, with absorption correction,

$$\frac{C_A}{C_B} = \frac{\delta_B}{\delta_A} \epsilon_{BA} \kappa_{BA} \frac{I_A}{I_B},$$

where the absorption correction is given by

$$\frac{\delta_B}{\delta_A} = \frac{\mu_{Alloy}^A}{\mu_{Alloy}^B} \frac{1 - \exp(-\mu_{Alloy}^B \theta f t_0)}{1 - \exp(-\mu_{Alloy}^A \theta f t_0)}$$

with $\mu_{Alloy}^A = \sum_{i=1}^N \mu_i^A C_i$,

μ_i^A = mass absorption coefficient of Element A in Element i (from tables),

C_i = approximate concentration of Element i, found from calculation without absorption,

ρ = density (g/cm³),

f = geometrical function of the take-off angle (θ) and beam angle of incidence (β), $\beta = 90^\circ$ for specimen perpendicular to beam.
 $= \sin \beta / \cos (\beta - \theta)$,

t_0 = thickness of foil in region where data are collected.

Of these variables, the densities ρ , θ , and μ are known or can be estimated, and C_i is estimated by the initial values obtained without any corrections. The thickness, however, is not known nor can it be easily measured. Thus, a range of thicknesses must be used to determine the absorption factors and a judgement made as to the best result based on physical considerations.

To estimate the importance of absorption for an element in an alloy, the Philibert-Tixier criterion is frequently used, which is given by

$$x_{pt} < 0.1,$$

where $x = \mu_{Alloy}^A f,$

μ_{Alloy}^A = mass-absorption coefficient of element A in the alloy

and f = geometrical factor.

For the case of Al, Ge, Sn, and Ti, the calculation of the above criterion and any subsequent absorption correction proceeds as follows:

- (1) Construct a table of μ_{Alloy}^A from element values given in the tables.¹⁰

		emitter→			
(Line)		(K)	(K)	(L)	(K)
Absorber		Al	Ge	Sn	Ti
+	Al	385.7	28	523.4	247
	Ge	7239.9	41.2	731.3	349.9
	Sn	6052.2	147.3	437.4	1232.1
	Ti	2288	115.4	231.1	110.6

- (2a) Calculate composite μ_{Alloy}^A for each element using

$$\mu_{Alloy}^A = \mu_{Ti}^{Al} C_{Al} + \mu_{Ge}^{Al} C_{Ge} + \mu_{Sn}^{Al} C_{Sn} + \mu_{Ti}^{Al} C_{Ti},$$

$$\mu_{Alloy}^{Al} = 2446.9608,$$

$$\mu_{Alloy}^{Ge} = 153.9087,$$

$$\mu_{Alloy}^{Sn} = 264.1247,$$

$$\mu_{Alloy}^{Ti} = 151.8181.$$

- (2b) Calculate absorption-criterion values for the element of interest, which is Al for this case. From (2a), $\mu_{\text{Alloy}}^{\text{Al}} = 2447$. For the alloy, $\rho = 4.5 \text{ g/cm}^3$. Thus, $\chi = f\mu = 1.08 (2447) = 2643$, and $\chi\rho = 11892$.

Hence, $\chi\rho t = 11892 t$, for t in cm. Therefore, if $t \leq 0.1 \mu = 1000 \text{ \AA}$, then absorption of radiation from Al in the alloy is negligible. Since the thickness range expected in the foils used may be larger than 1000° , a calculation of absorption is indicated.

- (3) Calculate absorption ratios assuming a 10^3 \AA thickness. The experimental parameters are

$$\theta = 32^\circ,$$

$$\beta = 90 - 35 = 55^\circ,$$

$$f = \frac{\sin 55}{\cos(55 - 32)} = 0.8899,$$

$$\rho = 4.5 \text{ g/cm}^3,$$

$$t_0 = 10^3 \text{ \AA} = 10^{-5} \text{ cm},$$

$$T = \rho f t_0 = 4.5(f) \cdot 10^{-5} = 4.005 \cdot 10^{-5}.$$

Thus, the absorption corrections are

$$\frac{\delta_{\text{Al}}}{\delta_{\text{Ti}}} = 0.9554,$$

$$\frac{\delta_{\text{c,n}}}{\delta_{\text{Ti}}} = 0.9977.$$

- (4) Calculate the ratios

(a) For the matrix,

$$\frac{C_{\text{Al}}}{C_{\text{Ti}}} = \frac{\delta_{\text{Ti}}}{\delta_{\text{Al}}} \frac{C_{\text{Al}}}{C_{\text{Ti}}} = \epsilon_K \frac{I_{\text{Al}}}{I_{\text{Ti}}} \frac{\mu_{\text{Ti}}}{\mu_{\text{Al}}} \frac{1 - \exp(-\mu_{\text{Al}}^{\text{Al}} T)}{1 - \exp(-\mu_{\text{Ti}}^{\text{Ti}} T)}$$

(b) For PPT plus matrix region, the matrix contribution is written as

$$\frac{C_{Al}}{C_{Ti}} = \frac{\delta_{Ti}^i}{\delta_{Al}^i} \frac{\kappa_{Ti}}{\kappa_{Al}} \frac{\epsilon_{Ti}}{\epsilon_{Al}} \frac{I_{Al}^i}{I_{Ti}^i} = \frac{\kappa_{Ti}}{\kappa_{Al}} \frac{\epsilon_{Ti}}{\epsilon_{Al}} \frac{I_{Al}^i}{I_{Ti}^i} \frac{\delta_{Ti}^i}{\delta_{Al}^i}$$

which yields, on solving for I_{Ti}^i ,

$$I_{Ti}^i = I_{Al}^i \frac{I_{Ti}^i}{I_{Al}^i} \frac{\delta_{Al}^i}{\delta_{Ti}^i} \frac{\delta_{Ti}^i}{\delta_{Ge}^i},$$

where $\delta_{Ti}^i/\delta_{Al}^i$ = absorption due to matrix, with thickness reduced by thickness of precipitate. The precipitate Ge intensity is written

$$\begin{aligned} I_{Ge}^i &= I_{Ti}^i \frac{\delta_{Ge}^i}{\delta_{Ti}^i} \frac{C_{Ge}}{C_{Ti}} \epsilon \kappa \\ &= I_{Ti}^i \frac{\delta_{Ge}^i}{\delta_{Ti}^i} \frac{\delta_{Ti}^i}{\delta_{Ge}^i} \frac{I_{Ge}}{I_{Ti}} \\ &= \frac{\delta_{Ge}^i}{\delta_{Ti}^i} \frac{\delta_{Ti}^i}{\delta_{Ge}^i} \frac{I_{Ti}^i}{I_{Ti}} I_{Ge} . \end{aligned}$$

Thus, the intensity for Ti and Ge due to the precipitate is

$$\begin{aligned} I_N(Ti) &= I_{Ti}'' - I_{Ti}^i , \\ I_N(Ge) &= I_{Ge}'' - I_{Ge}^i . \end{aligned}$$

The concentration ratios for the precipitate are given by

$$\frac{C_{Ge}}{C_{Ti_{ppt}}} = \frac{\delta_{Ti}''}{\delta_{Ge}''} \epsilon \kappa \frac{I_N(Ge)}{I_N(Ti)} ,$$

where $\frac{\delta_{Ge}''}{\delta_{Ti}''} = \left[\text{absorption due to} \right] \left[\text{absorption due to matrix} \right]$.

The matrix thickness is reduced by the thickness of the precipitate.
Hence, the reduced thickness is given by

$$T = \text{Thickness of matrix minus thickness of precipitate} \\ = \rho_{mx} f t_{mx} - \rho_{ppt} f t_{ppt}$$

For calculation purposes,

$$\begin{aligned} \text{estimate } \rho_{ppt} &= 5.0 \text{ g/cm}^3, \\ t_{mx} &= 1,000 \text{ \AA} = 10^{-5} \text{ cm}, \\ \text{and } t_{ppt} &= 100 \text{ \AA} = 10^{-6} \text{ cm}. \end{aligned}$$

This yields, on substitution into the equation for T,

$$T = 3.5560 \cdot 10^{-5},$$

and the absorption factor due to the presence of the precipitate is calculated to be

$$A_{\text{matrix}} = \frac{151.8181}{153.9087} \frac{1 - \exp(-153.9087 T)}{1 - \exp(-151.8181 T)} = 0.999963$$

which means that no appreciable absorption is occurring. The same calculation for the precipitate yields

$$A_{\text{ppt}} = 1.000272951$$

which means no absorption. Thus, the combined absorption factor is found to be

$$\frac{\delta_{\text{Ge}}''}{\delta_{\text{Ti}}''} = 1.00024.$$

Therefore, no absorption correction is needed for these thickness and size values. The only correction needed is in the initial Al value calculated for the matrix. Ge and Sn do not require corrections.

Summary

Ratios for matrix contribution to precipitate + matrix counts:

$$(a) \quad I_{Ti}' = \frac{I_{Al}'}{I_{Al}} I_{Ti} \frac{\delta_{Al}}{\delta_{Ti}} \frac{\delta_{Ti}'}{\delta_{Al}'} = \text{contribution of matrix to intensity}$$

$$(b) \quad I_{Ge}' = \frac{I_{Ti}'}{I_{Ti}} I_{Ge} = \text{contribution of matrix to intensity}$$

Net intensity due to precipitate:

$$(c) \quad I_N(Ti) = I_{Te}'' - I_{Ge}'$$

$$(d) \quad I_N(Ge) = I_{Ge}'' - I_{Ge}'$$

Concentration:

$$(e) \quad \frac{C_{Ge}'}{C_{Ti}'} = \frac{\epsilon_{Ti}}{\epsilon_{Ge}} \frac{\kappa_{Ti}}{\kappa_{Ge}} \frac{I_N(Ge)}{I_N(Ti)}$$

Conclusion

Absorption effects in the foil may be required when the foil thickness exceeds 0.1μ . Calculation of a corrected value of Al intensity leads, however, to a decrease in the weight percent calculated for Ge. The discrepancy remains unexplained at this time. Further corrections for fluorescence or atomic number may be required, but since methods for accomplishing such corrections are not well formulated and are the subject of research themselves, no further calculations were attempted.

The conclusion, based on Zaluszc's method as applied to the precipitates and on the electron diffraction data, is that the precipitate is Ti_5Ge_3 but that it may be slightly non-stoichiometric in composition.

Section 3
PAPERS, PRESENTATIONS, EXHIBITS,
MEETINGS, AND SCHOOLING

PAPERS AND PRESENTATIONS

1. "The Effect of Cooling Rate on the Microstructures of Rapidly Solidified (RST) Ti-6Al-4V," T. F. Broderick, A. G. Jackson, and F. H. Froes, in preparation.
2. "Microstructures of Rapidly Solidified Ti-5Al-2.5Sn with Si or Ge Additions," A. G. Jackson, T. F. Broderick, and F. H. Froes, Submitted for presentation at the 5th International Conference on Ti, Munich, Sept. 1984.
3. "Precipitation in Rapidly Solidified Ti-5Al-2.5Sn Containing Si and Ge Additions," A. G. Jackson, F. H. Froes, A. Clauer, and R. Carlomara, To be submitted to Met. Trans.
4. "On the Effect of NaCl on Porosity in Elemental-blend Powder Metallurgy Ti-5Al-2.5Sn," A. G. Jackson, F. H. Froes, and J. Moteff, To be published in Met. Trans.
5. "The Relationship Between Cooling Rate and Grain Size in RST Ti-6Al-4V," A. G. Jackson, T. F. Broderick, and F. H. Froes, Submitted for presentation at the TMS-AIME Annual Meeting, Los Angeles, CA, Feb. 1984.
6. "Microstructures of Rapidly Solidified Ti-6Al-4V and Beta III Alloys," T. F. Broderick, A. G. Jackson, and F. H. Froes, the Materials Research Society Meeting, Boston, MA, Nov. 1983.
7. "Analysis of Subprecipitates in Ti_5Si_3 in Aged Ti-5Al-2.5Sn-5Si," A. G. Jackson, F. H. Froes and J. Moteff, TMS-AIME Fall 1983 Meeting, Philadelphia, PA, Oct. 3, 1983.

8. "A BASIC Program for Calculating Zones and Planes in TEM Electron Diffraction Patterns," A. G. Jackson, TMS-AIME Fall 1983 Meeting, Philadelphia, PA, Oct. 3, 1983.
9. "A Modified Replication Technique to Study the Morphology of Cured Epoxy Resin," R. Omlor, V. B. Gupta, and L. T. Drzal, 41st Annual Meeting of the Electron Microscopy Society of America, Phoenix, AZ, Aug. 8-13, 1983.
10. "An Electron Microscopic Study of the Morphology of a Cured Epoxy Resin," R. Omlor, V. B. Gupta, L. T. Drzal, and W. W. Adams, Electron Microscopy Workshop on Polymers, Boston, MA, May 2-4, 1983; published in Conference Proceedings.
11. "A Study of the Microstructure Developed in Rapidly Solidified Ti-5Al-2.5Sn With Additions of Si and Ge," A. G. Jackson, Doctoral Dissertation submitted to the Department of Materials Science and Metallurgical Engineering, University of Cincinnati, Cincinnati, OH, Mar. 1983.
12. "Metallographic Studies of Consolidated Rapidly Solidified Titanium Alloys," P. R. Frausto, A. G. Jackson, A. H. Clauer, and J. L. McCall in Microstructural Science, Vol. 10 (Eds., W. White, J. Richardson, and J. McCall) (Elsevier Publishing Co., New York, 1982), p. 103.
13. "Effect of Aging on the Microstructure of Rapidly Cooled Ti-5Al-2.5Sn with Si Additions," A. G. Jackson, T. F. Broderick, F. H. Froes, and J. Moteff, Third Conference on Rapid Solidification Processing, Gaithersburg, MD, Dec. 6-9, 1982; published in Conference Proceedings.
14. "Composite Interphase Fracture: Effect of Graphite Fiber/Epoxy Matrix Adhesion," L. T. Drzal, M. J. Rich, and P. Lloyd, 13th Akron Polymer Conference on Fracture of Polymers and Composites, Akron, OH, May 21, 1982.

15. "Effect of Adhesion on the Interfacial Fracture Mode in Graphite Fiber-Epoxy Composites," L. T. Drzal, M. J. Rich, P. Lloyd, 5th Annual Meeting of the Adhesion Society, Mobile, AL, Feb. 22-24, 1982.
16. "Effects of Sintering on Porosity and Grain Size in PM Ti-5Al-2.5Sn," A. G. Jackson, F. W. Froes, and J. Moteff, Annual Meeting of the Metals Society of AIME, Dallas, TX, Feb. 15-17, 1982.
17. "Adhesion of Graphite Fibers to Epoxy Matrices: I. The Role of Fiber Surface Treatment," L. T. Drzal, M. J. Rich, and P. Lloyd, J. Adhesion 16, 1 (1982).
18. "Microstructures of Ti-5Al-2.5Sn Powder Material with High Si and Ge Content Prepared by the Pendant Drop Method," A. G. Jackson, R. Carbonara, A. Clauser, and F. H. Froes, Fall Meeting of AIME, Louisville, KY, Oct. 12, 1981.
19. "Gas-Gun Compaction Study of Ti Sponge," A. G. Jackson and F. Franta, Fall Meeting of AIME, Louisville, KY, Oct. 12, 1981.
20. "Interphase Effects on Fiber-Matrix Adhesion," L. T. Drzal, M. J. Rich, and P. Lloyd, Polymer Preprints 22(2), (1981), American Chemical Society Meeting, New York, NY, Aug. 1981.
21. "TEM Characterization of Aged Ti-5Al-2.5Sn Powder Metallurgy Alloys with Si and with Ge Additions," A. G. Jackson, R. E. Omlor, R. H. Froes, and J. Moteff, EMSA Annual Meeting, Atlanta, GA, Aug. 10-14, 1981.

22. "A Rapid Economical Method for Determining Locus of Fracture in Adhesive Bonded Joints," H. S. Schwartz and R. J. Bacon, AIAA 22nd SDM Conference, Atlanta, GA, Apr. 6-8, 1981; published in Conference Proceedings.
23. "Staining Behavior and Morphology of ABPBI/PBT Polymer Blends and Alloys," P. Lloyd, R. E. Omlor, A. K. Kulshreshtha, and D. R. Wiff, Pittsburgh Conference on Analytical Chemistry and Applied Spectroscopy, Atlantic City, NJ, Mar. 9-13, 1981; published in Conference Proceedings.
24. "Techniques for Preparation of Prealloyed Metal Powder for Examination by Transmission Electron Microscopy," P. F. Lloyd, R. E. Omlor, and L. E. Matson, Pittsburgh Conference on Analytical Chemistry and Applied Spectroscopy, Atlantic City, NJ, Mar. 9-13, 1981; published in Conference Proceedings.
25. "Morphological and Microstructural Evaluation of Various Titanium Alloy Powders," R. E. Omlor, R. J. Bacon, D. Eylon, and F. H. Froes, AIME Symposium on Titanium Powder Metallurgy, Las Vegas, NV, Feb. 26-28, 1980; published in the Conference Proceedings.
26. "Microstructure Property Correlation in Cold-Pressed and Sintered Elemental Ti-6Al-4V Powder Compacts," Y. Mahajan, D. Eylon, R. J. Bacon, and F. H. Froes, 109th AIME Annual Meeting of the Metallurgical Society, Las Vegas, NV, Feb. 26-28, 1980; published in Conference Proceedings.

EXHIBITS

1. "Inconel 'Eruption'," F. Vahldiek and E. Harper, International Metallographic Society Symposium and Technical Workshop and Metallographic Exhibit, Calgary, Alberta, Canada, July 18-22, 1983.

2. "Removing Residual Surface Stress of Ti-6Al-2Sn-4Zr-6Mo," E. Harper and J. Larsen, International Metallographic Society Symposium and Technical Workshop and Metallographic Exhibit, Calgary, Alberta, Canada, July 18-22, 1983.
3. "Contamination of X7091 Al P/M Alloy," S. Mazdiasni, C. Heidenreich, and J. Paine, International Metallographic Society Symposium and Technical Workshop and Metallographic Exhibit, Orlando, FL, July 21-24, 1982.
4. "Hammer Forged IMI-829," S. Fujishiro and R. Lewis, International Metallographic Society Symposium and Technical Workshop and Metallographic Exhibit, Orlando, FL, July 21-24, 1982.
5. "Microstructure of Hyperperitectic Ti-28 wt% W," S. Krishnamurthy, J. Paine and F. Deutscher, International Metallographic Society Symposium and Technical Workshop and Metallographic Exhibit, Orlando, FL, July 21-24, 1982.
6. "Localized Grain Refinement," M. Cook and E. Harper, International Metallographic Society Symposium and Technical Workshop and Metallographic Exhibit, Orlando, FL, July 21-24, 1982.
7. "Titanium Matrix Composites," P. Smith and B. Strobe, International Metallographic Society Symposium and Technical Workshop and Metallographic Exhibit, Orlando, FL., July 21-24, 1982.
8. "Metal Powder Preparation for TEM by Electrolytic Codeposition," G. Staniek and E. Harper, International Metallographic Society Symposium and Technical Workshop and Metallographic Exhibit, Orlando, FL, July 21-24, 1982.

9. "Pack Man," G. Staniek, R. Omlor, and E. Harper, International Metallographic Society Symposium and Technical Workshop and Metallographic Exhibit, Orlando, FL, July 21-24, 1982.
10. "Organosilicon-Infiltrated Porous Reaction Sintered Si_3N_4 ," D. Bierman, K. Mazdiyasni, and P. Lloyd, International Metallographic Society Symposium and Technical Workshop and Metallographic Exhibit, Orlando, FL, July 21-24, 1982.
11. "Oxidation Scale of Hot Pressed Silicon Nitride with Cerium Compound as Densification Aid," D. Bierman, T. Mah, and M. Rowe, International Metallographic Society Symposium and Technical Workshop and Metallographic Exhibit, Orlando, FL, July 21-24, 1982.
12. "Ti-13V-11Cr-3Al, Cp-Ti, Ti-5Al-2.5Sn, Ti-6Al-6V-2Sn Extrusion," I. Martorell and S. Nash, International Metallographic Society Symposium and Technical Workshop and Metallographic Exhibit, Orlando, FL, July 21-24, 1982.
13. "Complex Extrusion," I. Martorell, M. Myers, and E. Harper, International Metallographic Society Symposium and Technical Workshop and Metallographic Exhibit, Orlando, FL, July 21-24, 1982.
14. "Graphite Fiber-Epoxy Interfacial Failure Analysis," L. T. Drzal, A. Bierman, and P. Lloyd, IMS AIME Fall Meeting, Louisville, KY, Oct. 11-15, 1981; Traveling Exhibit, American Society of Metals, Honorable Mention.

15. "Microscopic Characterization Structural Adhesive Joint Interphase," L. T. Drzal, A. Bierman, P. F. Lloyd, and R. Omlor, Displayed at the 1981 Metallographic Exhibit during the International Metallographic Meeting, San Francisco, CA, July 19-22, 1981. Winner of second-place award in the analytical category. Displayed in Traveling Exhibit sponsored by the American Society of Metals in Cincinnati, OH, and Louisville, KY.
16. " $Ti_3Al(Nb)/Ti-6Al-4V$ Composite," B. Strobe and R. J. Bacon, IMS Metallographic Exhibition, International Metallographic Meeting, Brighton, England, Aug. 18-22, 1980.

MEETINGS AND SEMINARS ATTENDED

1. Electron Microscopy Society of America/Microbeam Analysis Society, Phoenix, AZ, Aug. 8-12, 1983.
2. International Metallography Society Metallographic Exhibition, Calgary, Canada, July 18-21, 1983.
3. Electron Microscopy Society of America/Microbeam Analysis Society, Washington, D.C., Aug. 8-23, 1982.
4. International Metallography Society Metallographic Exhibition, Orlando, FL, July 17-20, 1982.
5. Powder Seminar at Wright-Patterson Air Force Base, OH, June 4, 1982.
6. Joint Conference, American Institute of Aeronautics and Astronautics, American Society of Mechanical Engineers, American Society of Civil Engineers and American Helicopter Society, Atlanta, GA, Ap. 6-8, 1981.

7. Pittsburgh Conference on Analytical Chemistry and Applied Spectroscopy, Atlantic City, NJ, Mar. 9-13, 1981.
8. Electron Microscopy Society of America Microbeam Analysis Society, Reno, NV, Aug. 4-8, 1980.

SCHOOLS ATTENDED

1. R. Omlor, Tracor Northern TN-2000 Training School, Madison, WI, Oct. 31 - Nov. 5, 1982.
2. R. Omlor, 100 CX Microscope School, Boston, MA, Dec. 13-18, 1981.
3. B. Brodecki and R. Bacon, Scanning Electron Microscopy and X-Ray Microanalysis, Lehigh University, Bethlehem, PA, June 8-12, 1981.

REFERENCES

1. "Airplane Damage Tolerance Requirements," Military Specification MIL-A-83444 (U.S. Air Force, 1974).
2. "Airplane and Strength and Rigidity, Reliability Requirements, Repeated Loads and Fatigue," Military Specification MIL-A-8867 (U.S. Air Force, 1975).
3. J. L. Racich and J. A. Koutsky, J. Appl. Polym. Sci. 20, 2111 (1976).
4. J. P. Bell, J. Appl. Polym. Sci. 27, 3503 (1982).
5. M. D. Skibo, et al., J. Mater. Sci. 11, 679 (1976).
6. W. J. Paradee "Quantitative Nondestructive Evaluation (NDE) For Retirement for Cause," TR No. 1, Sept. 29, 1980, through Sept. 28, 1981 (Rockwell International Science Center, Thousand Oaks, CA).
7. K. Puhl, Mater. Sci. Eng. 1, 313 (1967).
8. L. Katgerman, Scripta Met. 14(8), 861 (1980).
9. J. Hren, J. Goldstein, and D. Joy, Introduction to Analytical Electron Microscopy, Chapters 3-4, (Plenum Press, NY, 1979).
10. T. O. Ziebold, Editor, Lecture Notes on "The Electron Microanalyzer and its Applications" (M.I.T., Cambridge, MA, 1969).

APPENDIX

POROSITY AND GRAIN GROWTH IN PM Ti-5Al-2.5Sn WITH Si AND Ge

A. G. Jackson
Systems Research Laboratories, Inc.
Dayton, Ohio

F. H. Froes
AFWAL, Materials Laboratory
Wright-Patterson Air Force Base, Ohio

J. Moteff
University of Cincinnati
Cincinnati, Ohio

ABSTRACT

Ti-5Al-2.5Sn alloy with varying amounts of Si or Ge and produced by the blended elemental process showed high porosity volume fraction even after extended sintering in vacuum at 1315°C. The volume fraction was approximately proportional to solute content. Grain growth for the base alloy was proportional to $t^{1/3}$ but, with increasing solute content, the growth curve departed from a simple $t^{1/3}$ behavior. The interaction of the porosity with grain boundaries and the type of microstructure contribute to this complex behavior.

INTRODUCTION

The preparation of Ti alloys from powder using an elemental blend offers the potential of making near-net-shapes economically, thus providing a cost-savings in the use of Ti. The process has been successfully applied to Ti-6Al-4V; this alloy has been studied extensively, while other Ti alloy formulations have received little attention. The purpose of this work was to examine a Ti alloy prepared by the blended elemental process in terms of its porosity and grain-growth behavior.

The alloy studied was the near-alpha Ti-5Al-2.5Sn with additions of Si and of Ge. The alloys examined are listed in Table 1. The range of concentrations cover solid-solubility limits in the alpha and the eutectic/eutectoid range for the high concentrations. The alloys were prepared from a true elemental blend of Al and Sn powder and electrolytic Ti sponge by cold compacting and then sintering at 1315°C for 4 hr.* This temperature lies in the beta-phase field and is only a few hundred degrees below the liquidus for all of the alloys studied. These additions are reported to be potent strengtheners in conventionally formulated alloys and were chosen to verify their expected large effect upon the mechanical properties of the material.

Since the alloys under study contained volume fractions which ranged from 10% to > 40%, applications involving fatigue-limited forms related to airframes and engine components were not feasible. Consequently, procedures were chosen which would permit determination of whether continued sintering

* By Gould Laboratories, Cleveland, OH

Table 1
WEIGHT PERCENT OF
COMPONENTS IN ALLOYS STUDIED

Ti	Al	Sn	Si	Ge
92.5	5.0	2.5		
92.5	4.99	2.40	0.1	
92.5	4.98	2.49	0.5	
91.6	4.95	2.48	.99	
88.1	4.76	2.38	4.76	
84.1	4.55	2.27	9.09	
80.4	4.34	2.17	13.0	
92.5	4.99	2.49	-	0.1
92.0	4.98	2.49	-	.49
91.6	4.95	2.48	-	.99
91.1	4.93	2.46	-	1.48
86.1	4.65	2.33	-	6.98
80.4	4.34	2.17	-	13.0
75.5	4.08	2.04	-	18.4

Nominal additions to Ti-5Al-2.5Sn (in wt. percent)

Si 0.1, 0.5, 1.0, 5.0, 10.0, 15.0

Ge 0.1, 0.5, 1.0, 1.5, 7.5, 15.0, 22.5

would significantly reduce the pore volume fraction to levels acceptable for fatigue uses. Therefore, the sintering temperature chosen was the same as that used in the compacting-sintering process. If extended sintering at 1315°C yielded good results, then further tests of the alloys for mechanical properties could be made.

The results reported here include the changes in porosity and the growth of grains in the alloys as a result of the simple sintering procedure described above.

EXPERIMENTAL

The as-received alloys were in the form of ~ 80-gm bars 9.5 mm square and ~ 76mm long. Specimens were cut from the bars and polished to reveal either the pore structure or the grain structure. These samples were encapsulated in Epomet, ground to a 600 SiC grit finish, intermediate polished on nylon cloth with 6- μ diamond paste, and final polished in the vibratory polisher on microcloth in a 0.3- μ alumina slurry. The samples were then etched in a solution of 10 ml 40% KOH, 5 ml H₂O₂ (30%), and 20 ml H₂O. The samples were observed optically, and polarized microphotographs were recorded. Sets of specimens were then vacuum sintered for 10, 30, and 50 hr. at 1315°C.

Porosity was determined by use of an electronic planimeter which measured the pore area fraction present in a series of micrographs. At least 18 data points were taken for each specimen per sintering treatment.

Grain size was measured by the linear-intercept method. Again 18 measurements per specimen per sintering treatment were made to determine the spread in the data.

RESULTS

The pores in the as-received material had a ragged shape but were not interconnected. Thus, the alloys had been sintered to the intermediate stage. In all alloys studied, the pore morphology showed noticeable changes with time at temperature, indicating that the intermediate stage had transformed to the final stage as characterized by rounded pore shape and many pores located within grains. A significant number of pores, however, remained at the grain boundaries.

Several of the alloys could not be studied because of the large pore volume fraction. The 15 wt pct Si alloy sintered poorly and crumbled easily. The 5 wt pct and 10 wt pct Si alloys exhibited noticeable decrease in porosity with time at temperature, but the volume fraction remained high even after the 50-hr treatment. Grain-size measurement in these alloys was not possible, nor was an accurate measurement of f_v possible except in the 5 wt pct Si case after 10-hr exposure at temperature. The high solute Ge alloys also sintered poorly, forming compounds during the extended sintering period.

Porosity

The base-alloy behavior was as expected in terms of a decrease in f_v . The volume fraction decreased linearly on a log-log plot, as shown in Fig. 1.

The slope of this curve indicates a relationship of the form

$$f_v \propto t^{-1/6}.$$

The Si alloy behavior is shown in Fig. 2. The lowest solute alloy exhibits a decline in f_v with time up to 30 hr, at which time a marked increase occurs. The 0.5Si alloy exhibits an initial increase, followed by a decrease. This is probably related to the transformation from the intermediate to the final stage in the sintering process. Changes in microstructure are noted at 30 hr which suggests that strong interaction between pores and grain boundaries is occurring. The 1 wt pct Si alloy exhibits a relatively flat curve up to 30 hr, at which time a decrease is noted. This again is believed to be related to the change in microstructure. The 5 wt pct Si f_v data show that large and rapid changes occur initially after 30 hr, indicating that this alloy may have been in the late stages of initial sintering in the as-received condition. Upon further sintering, through the intermediate stage to the final stage, the pore volume decreased slowly until the change in microstructure occurred, allowing pore volume to decrease rapidly.

The Ge alloy behavior, shown in Fig. 3, was somewhat more regular than that of the Si alloys. The 0.1 wt pct Ge alloy displayed slowly decreasing f_v . The 0.5 and 1 wt pct Ge alloys exhibited an initial increase in f_v at 10 hr, followed by a slow decrease in f_v . As in the Si alloy cases, the transformation from the intermediate to the final stage of sintering, and the microstructural changes at 30 hr are responsible for this behavior. The 1.5 wt pct Ge alloy exhibited a relatively steady value for f_v , a slight drop being noted after 30 hr. The 7.5 wt pct Ge alloy, for which f_v was very high initially, exhibits a rapid decrease in f_v between 10 and 30 hrs, followed

by a large drop to a steady value at 30 hr and beyond. The 15 wt pct Ge alloy yielded consistently high values for f_v , with no decrease up to 50 hr.

The micrographs in Fig. 4 display the typical porosity changes which occur over the four time periods studied. The alloy in this figure is the 0.1Si alloy, but it is representative of all the alloys studied. Notice the change from an irregular shape and distribution to one which is well rounded. Size distributions were not measured, but qualitatively the distribution changes remarkably to one having a very narrow width of diameters. On the average, small and very large pores have been consolidated into a narrow band of diameters.

GRAIN GROWTH

Grain growth in the alloys was complex except in the case of the base material, where a $t^{1/3}$ law was obeyed. Additions of solute affected the behavior in proportion to the level of solute added. The net effect was to impede the grain growth until the grain boundaries broke away from pores, whereupon rapid growth occurred.

The base-alloy grain-growth curve is shown in Fig. 5. The growth is regular and has a slope of 0.33. This type of growth is expected in a well-behaved material and corresponds to the decrease in f_v noted earlier.

The Si-containing alloys showed complex behavior, as illustrated in the curves in Fig. 6. The effects of solute level can be seen. The growth in the lowest solute alloy (0.1 wt pct Si) was similar to that in the base alloy up to 10 hr, at which time a leveling occurred up to 30 hr. The 0.5 wt pct Si alloy exhibited similar growth. After 30 hrs, the rate increased dramatically.

Since a large microstructural change occurred at this time, as explained above, the source for this variation in growth is believed to be related to this change. The 1 wt pct Si material exhibited a flat growth rate up to 30 hr. at which time the rate increased noticeably.

In the Ge alloys, (Fig. 7) the effects of solute concentration are more dependent than in the case of the Si alloys. The 0.1 Ge alloy curve deviates slightly from the base-alloy curve, exhibiting a steadily increasing rate. The 0.5 and 1 wt pct Ge alloys follow the base-alloy behavior up to 30 hr, at which time the rate drops. This is followed by a large increase in size, indicating rapid growth.

Microstructures for the alloys studied are illustrated in Fig. 8 for the 0.1 wt pct Si alloy. These are typical of the microstructures of the alloys in which grain structure was measureable. The initial structure is α but is not well equiaxed. This structure is observed at 10 hr as well; but at 30 hr, plate-like grains become evident. These are well developed at 50 hr. Such microstructures compare well with those observed in conventionally prepared Ti-5Al-2.5Sn which has been heated in the β and then cooled to form α .

DISCUSSION

Porosity in these blended elemental alloys is high and is not reduced to levels acceptable for use in fatigue-limited applications by simple extension of the sintering parameters used during the consolidation process. The volume fraction-time relationship is complex except for the base alloy, where a decrease proportional to $t^{-1/6}$ is noted.

The addition of solute (Si or Ge) has a strong effect upon the volume-fraction kinetics, probably because of the solute drag produced. This relationship, however, is not simple. The effect of adding solutes appears to extend the time required for sintering to take place.

Grain growth in the base alloy proceeds according to a $t^{1/3}$ law. Addition of a solute produces a decrease in the kinetics which is roughly proportional to the amount of solute present. A breakaway in grain growth occurs after extended sintering. The growth rate becomes high, rapidly increasing the grain size. The behavior of this high-growth-rate portion of the sintering is not clear. It may be a catch-up process, i.e., the rate increases rapidly until the grain size reaches values comparable to those of the base material, after which the rate decreases to that of the base alloy. The rate may continue to be high, leading to a rapid growth in grains to sizes comparable to those in conventional alloys. The data presented are not definitive on this point. The grain sizes measured are very small, as compared with those developed in alloys prepared by conventional procedures (cast, forged, wrought, swaged, etc.), indicating that the effects of PM approaches on grain size apply in this system. For this alloy system, additional processing is required to reduce the porosity to levels of a few volume percent or less. Processes such as HIPing or vacuum hot pressing are appropriate candidates.

CONCLUSIONS

This study has shown that a simple extension of the sintering process used in producing the compact is ineffective in reducing porosity without an attendant large increase in grain size.

This work has further shown that after additional processing compacts can be produced which may be useful in fatigue limited applications. Even unprocessed, these compacts can be used as source material for producing prealloyed powders. In this case, advantage is taken of the PM property of combining alloying elements to produce alloys not possible through the use of melt techniques.

The study also points out the danger in assuming that processes applicable to an alloy system such as Ti-6Al-4V are applicable to a related system.

LIST OF FIGURES

Figure

- 1 Area fraction versus sintering time at 1315°C for base alloy.
- 2 Area fraction versus sintering time for base alloy with various amounts of Si.
- 3 Area fraction versus sintering time for base alloy with various amounts of Ge.
- 4 Porosity obtained in base + 0.1 wt pct. Si alloy: (a) as-received, (b) after 10 hr at 1315°C; (c) after 30 hr; (d) after 50 hr.
- 5 Grain size (mm/grain) versus sintering time for base alloy.
- 6 Grain size (mm/grain) versus sintering time for Si containing alloys.
- 7 Grain size (mm/grain) versus sintering time for Ge containing alloys.
- 8 Microstructures obtained in base + 0.1 wt pct. Si alloy: (a) as-received, (b) after 10 hr at 1315°C; (c) after 30 hr; (d) after 50 hr. Note the change from equiaxed α to plate-like α' .

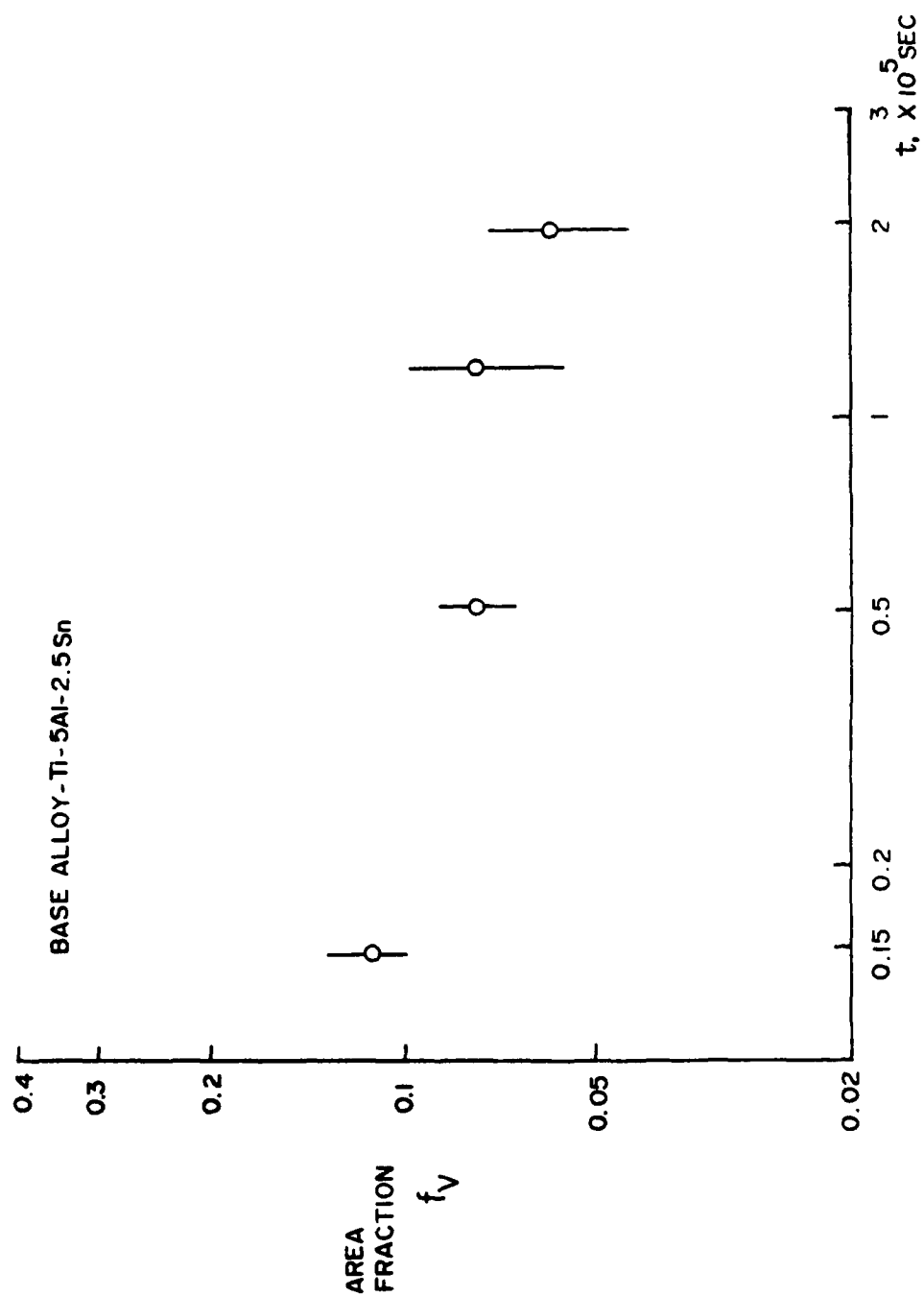


Figure 1. Area Fraction Versus Sintering Time at 1315°C for Base Alloy.

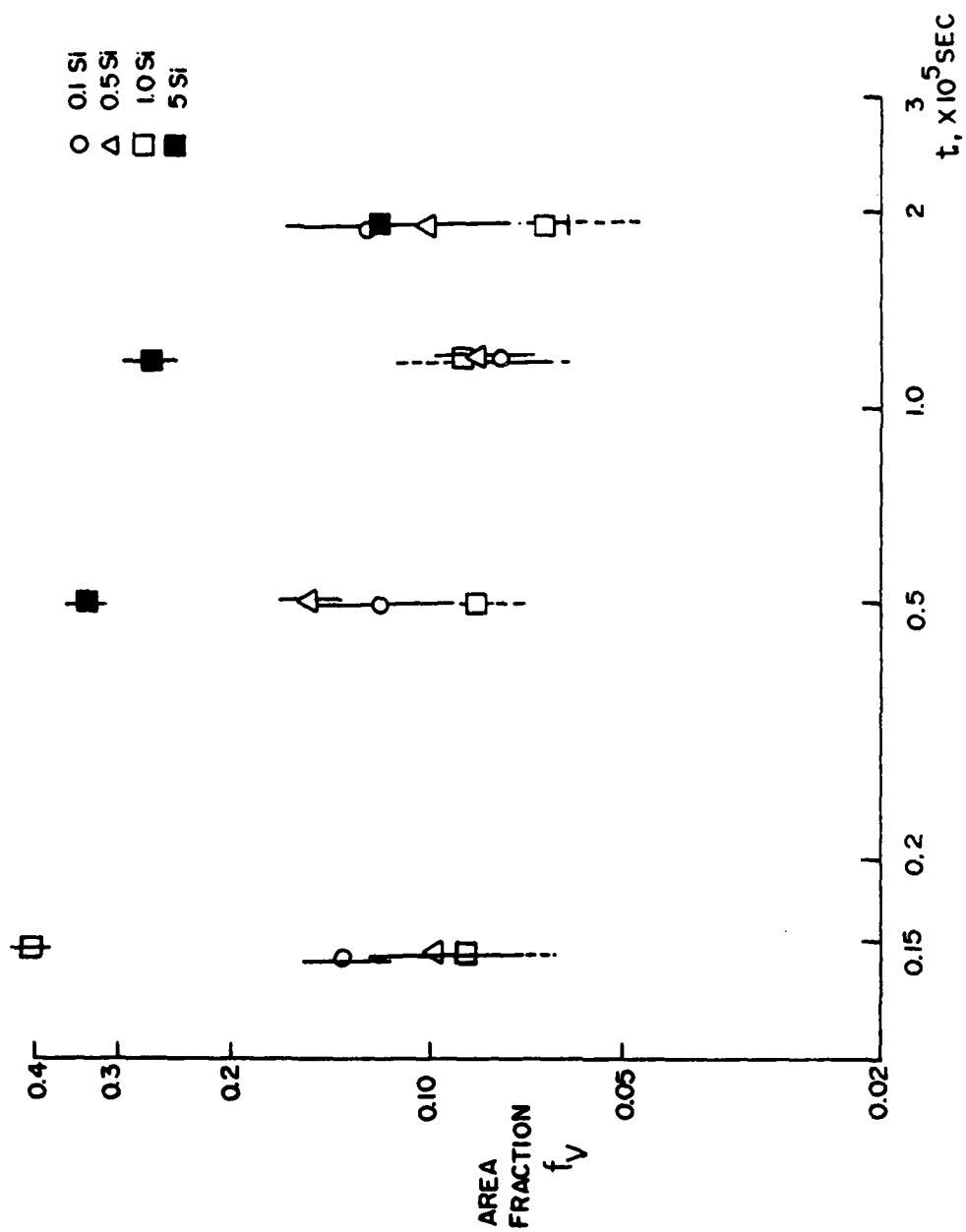


Figure 2. Area Fraction Versus Sintering Time for Base Alloy With Various Amounts of Si.

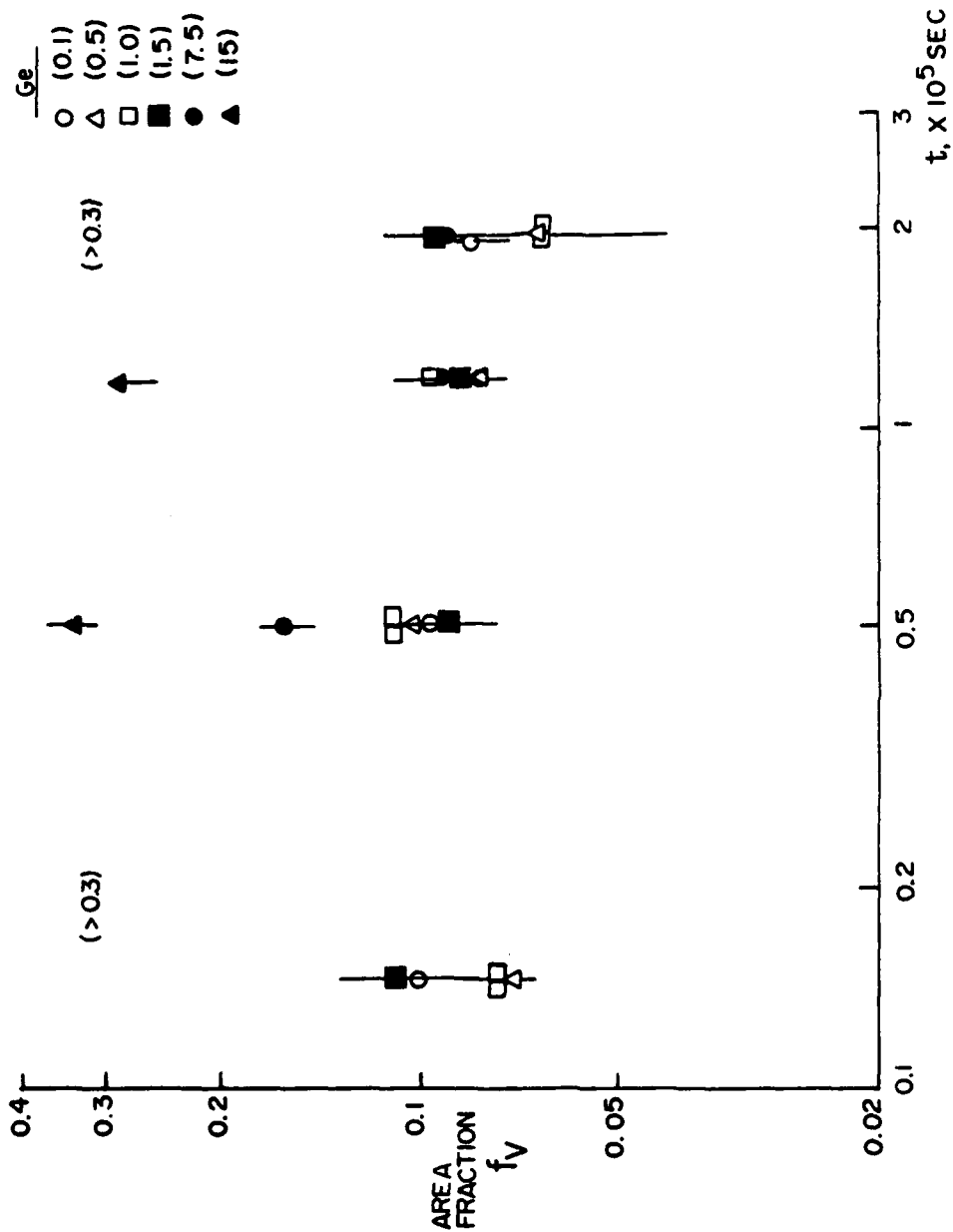


Figure 3. Area Fraction Versus Sintering Time for Base Alloy with Various Amounts of Ge.

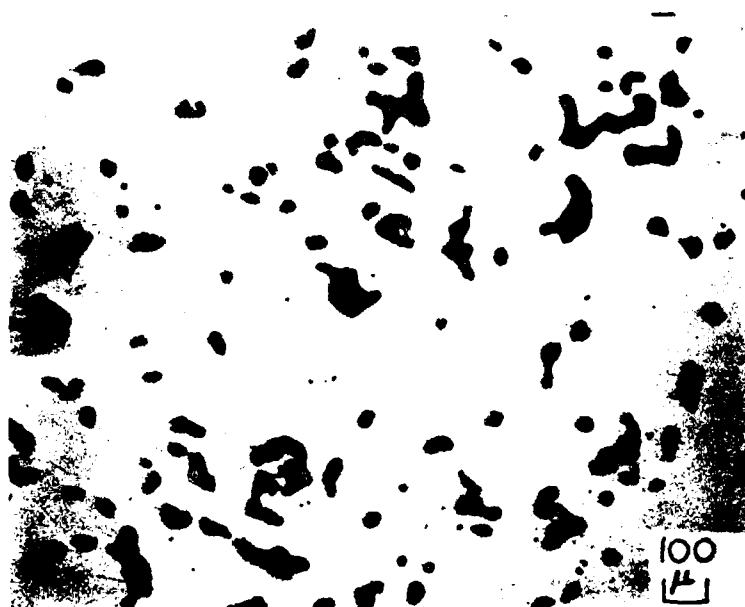
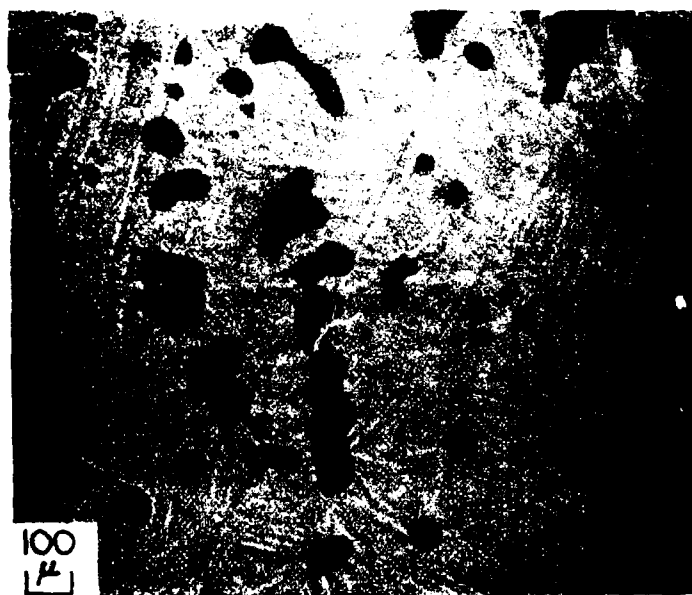


Figure 4. Porosity Obtained in Base + 0.1 wt. pct. Si Alloy: (a) As-Received, (b) After 10 hr. at 1315°C, (c) After 30 hr., (d) After 50 hr.



(c)



(d)

Figure 4 (Continued)

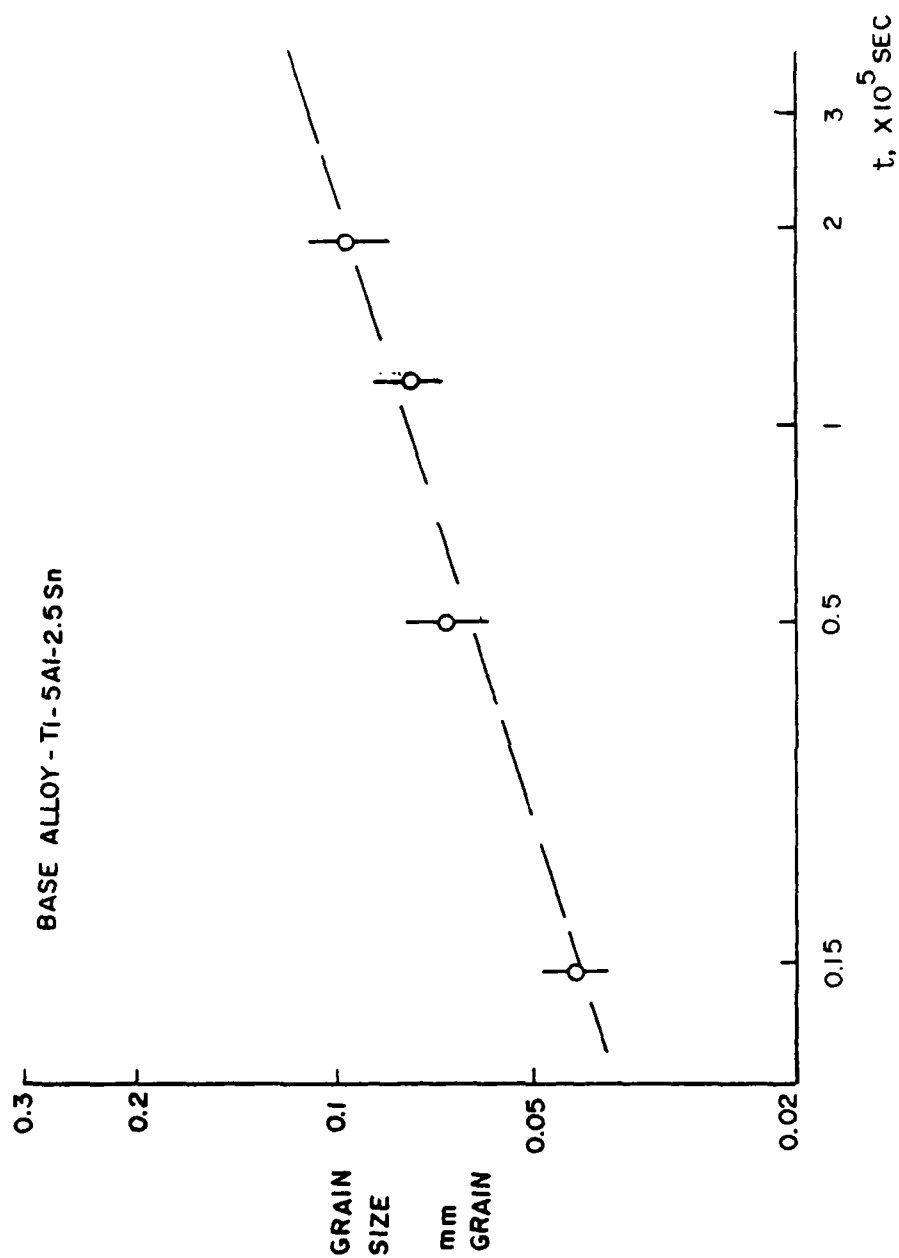


Figure 5. Grain Size (mm/Grain) Versus Sintering Time for Base Alloy.

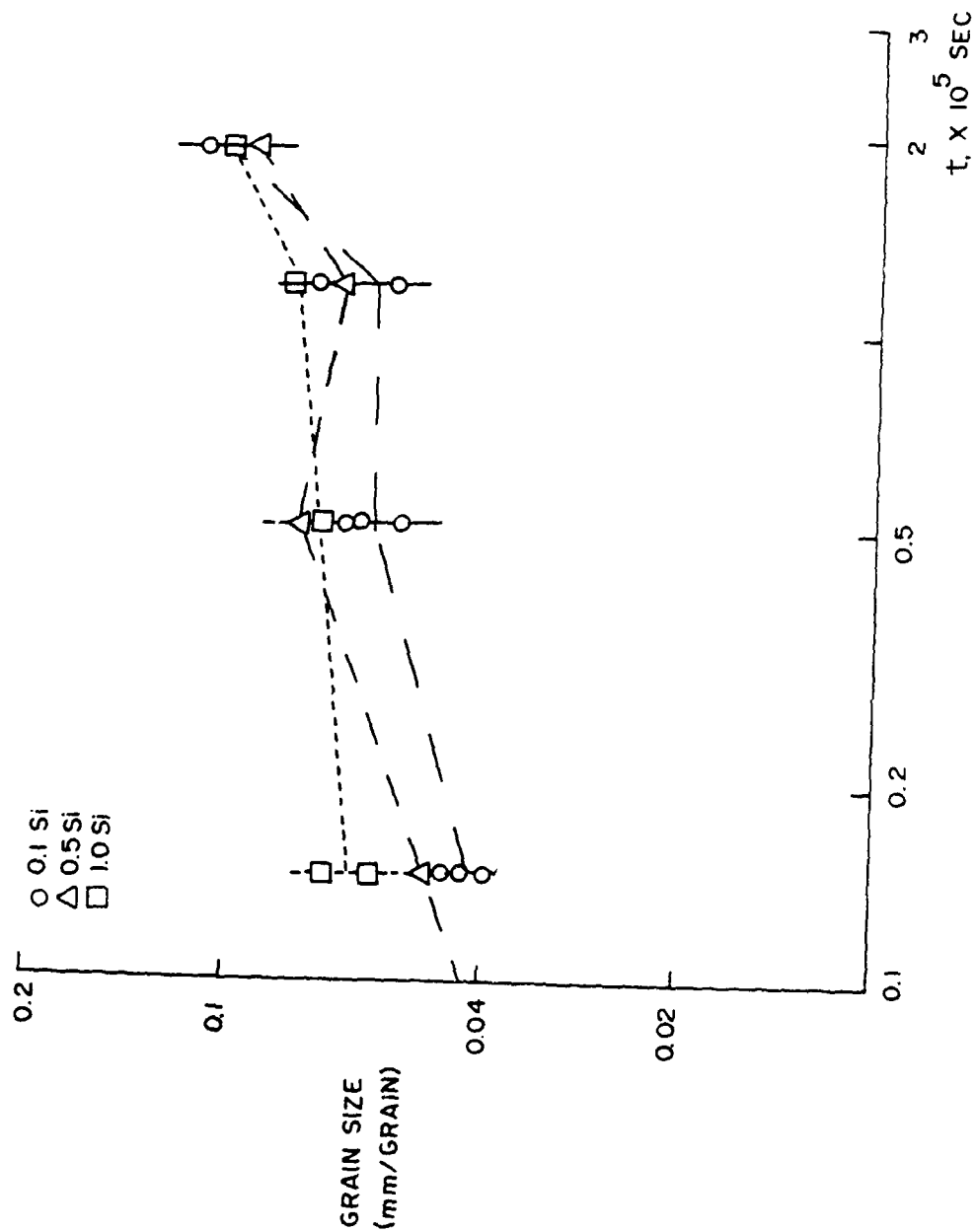


Figure 6. Grain Size (mm/Grain) Versus Sintering Time for Si Containing Alloys.

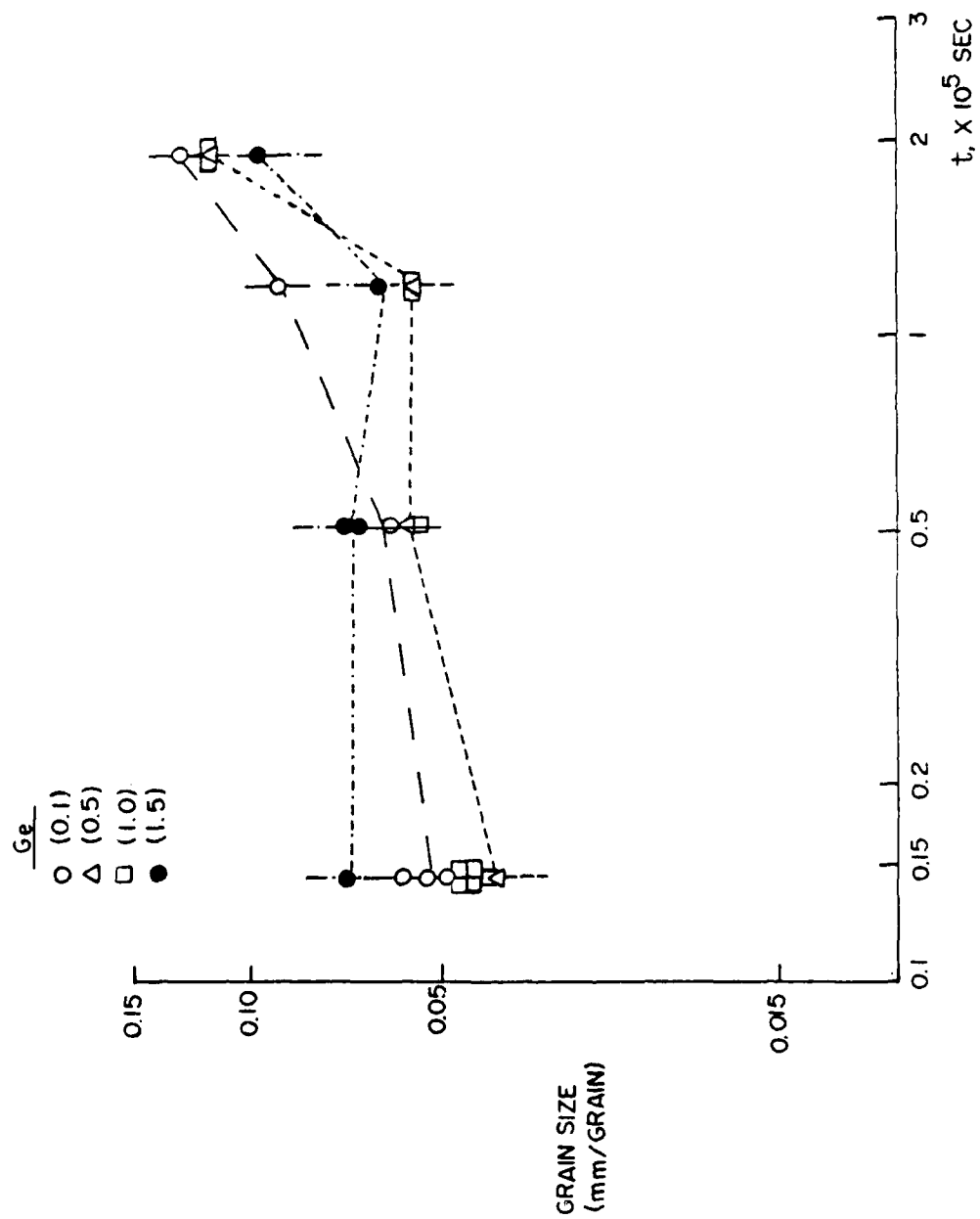


Figure 7. Grain Size (mm/grain) Versus Sintering Time for Ge Containing Alloys.

AD-A141 946

CHARACTERIZATION OF THE MICROSTRUCTURES OF VARIOUS
MATERIALS(U) SYSTEMS RESEARCH LABS INC DAYTON OH
RESEARCH APPLICATIONS DIV A G JACKSON ET AL. APR 84
AFWAL-TR-84-4052 F33615-80-C-5079

2/2

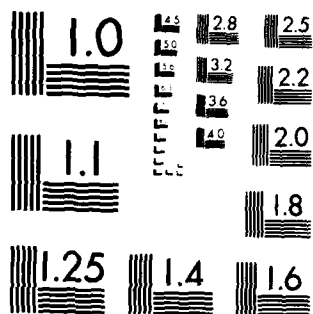
UNCLASSIFIED

F/G 11/6

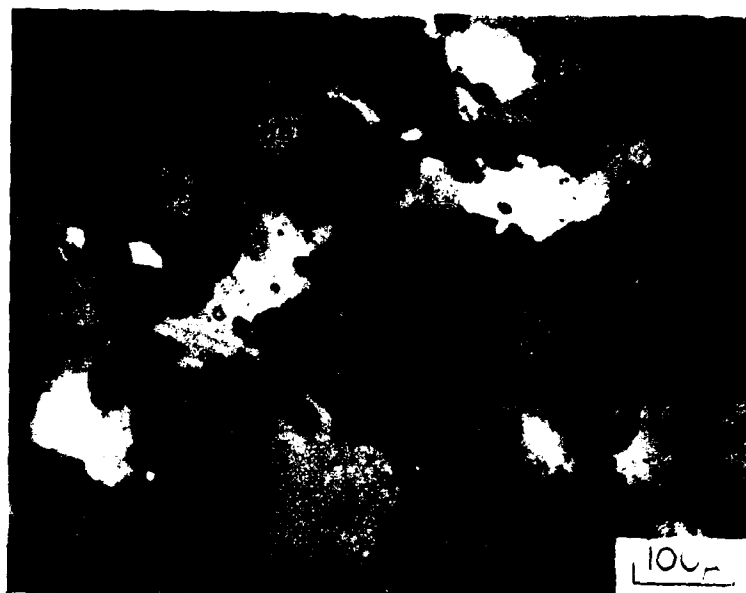
NL



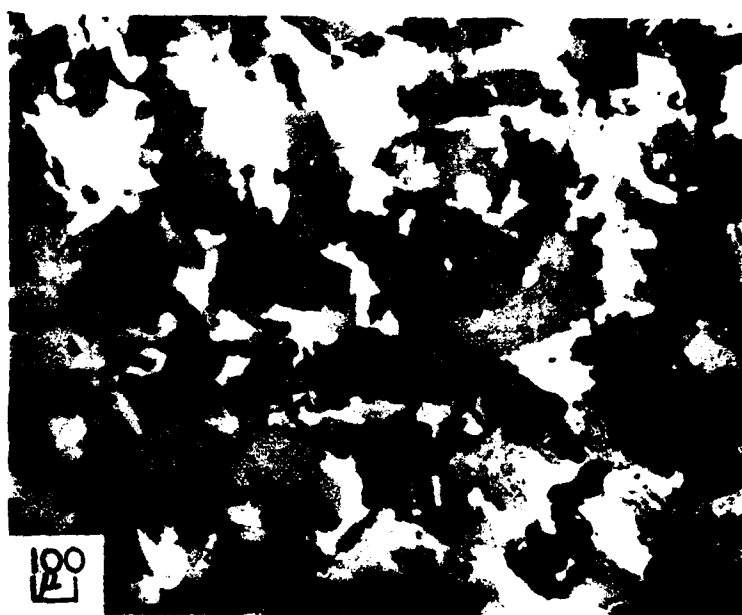
END
DATE
FILMED
7 84
DTIC



MICROCOPY RESOLUTION TEST CHART
NATIONAL BUREAU OF STANDARDS-1963-A

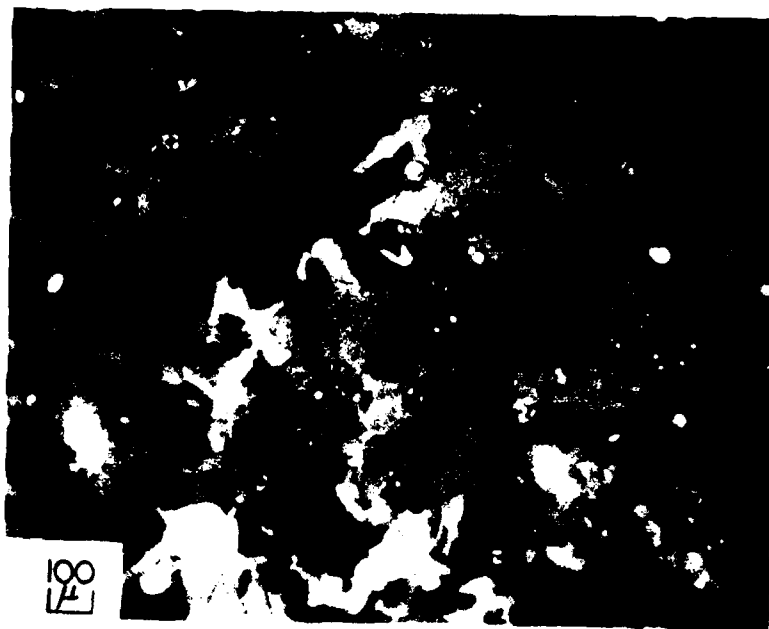


(a)



(b)

Figure 8. Microstructures Obtained in Base + 0.1 wt. pct. Si Alloy: (a) As-Received, (b) After 10 hr. at 1315°C, (c) After 30 hr., (d) After 50 hr. Note the change from equiaxed α to plate-like α' .



(c)



(d)

Figure 8 (Continued)